Radiation belts of the Earth: overview, methods of investigation, recent observations on the CORONAS-Photon" spacecraft

O.V. Dudnik[1] , J. Sylwester[2] , P. Podgorsky[2] , S. Gburek[2]

[1] V.N. Karazin Kharkiv National University, Ukraine
E-mail: Oleksiy.V.Dudnik@univer.kharkov.ua

[2] Solar Physics Division, Space Research Center, Polish Academy of Sciences
E-mail: js@cbk.pan.wroc.pl; pp@cbk.pan.wroc.pl; sg@cbk.pan.wroc.pl

Magnetosphere and radiation belts

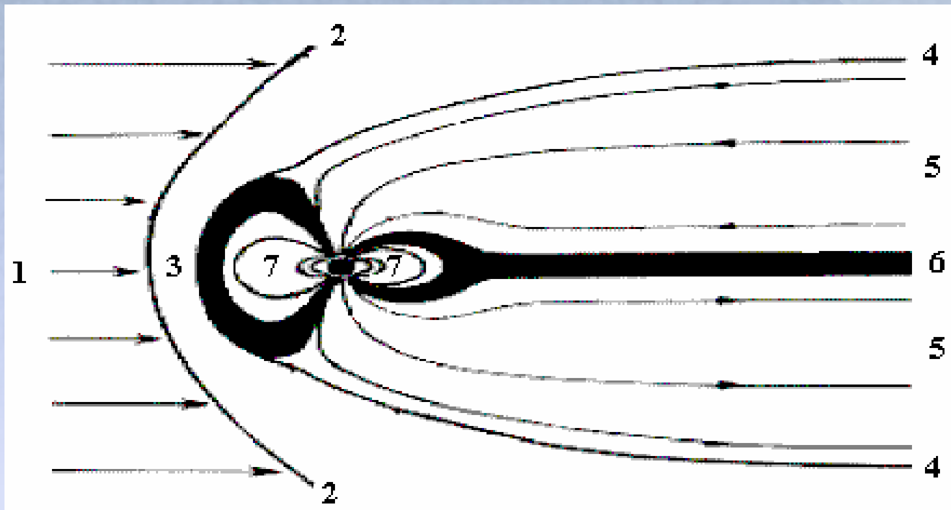

1 - solar wind;
2 - bow shock;
3 - magnetosheath – turbulent region;
4 - magnetopause - outer border of magnetosphere;
5 - magnetotail: North lobe and Sourth lobe, plasma mantle;
6. - plasma sheet;
7. - geomagnetic trap with particles of radiation belts and ring current

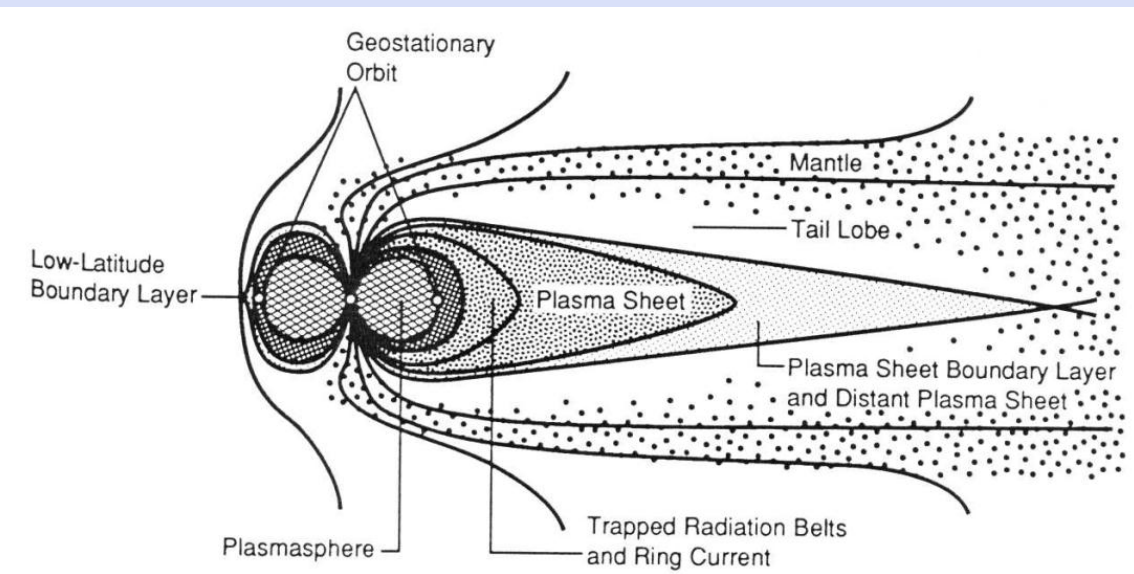

Plasma regions of the magnetosphere.
Schematic drawing of the most important plasma regions of the magnetosphere as seen in the noon-midnight meridian plane.
Solid lines are magnetic field lines.

Kivelson, M. G., Russell, C. T. (eds.) 1995, Introduction to Space Physics, Cambridge University Press, Cambridge, United Kingdom

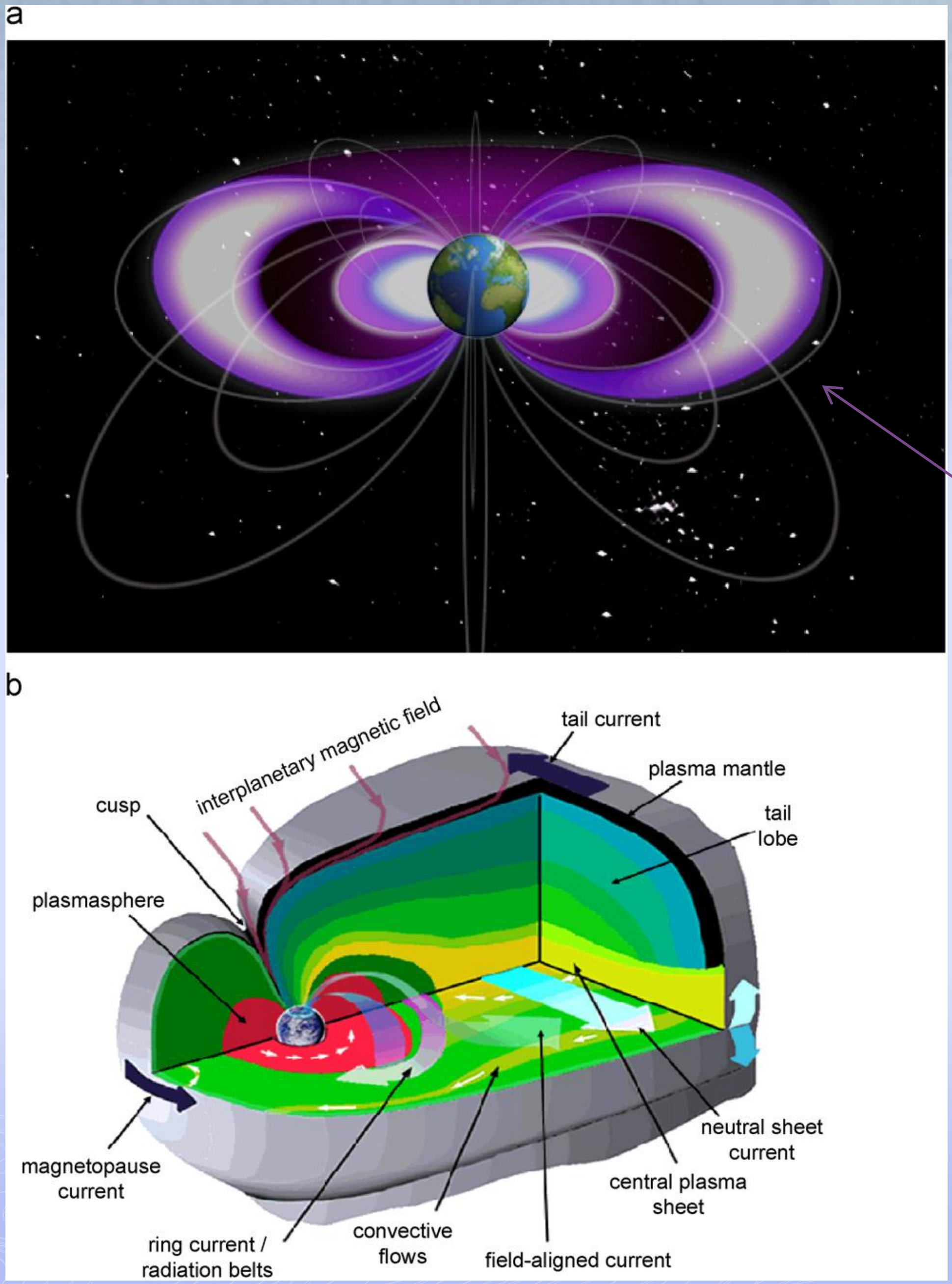

Classic view of the Van Allen radiation belts showing a two-belt structure with slot region.

The inner belt, first discovered by Explorer 1 in 1958, is primarily populated by protons produced by cosmic ray albedo neutron decay, with a contribution from solar energetic proton trapping.

The outer belt is populated by electrons with a plasma sheet source (b)

Mary K. Hudson,, Brian T. Kress, Hans-R. Mueller, Jordan A. Zastrow, J. Bernard Blake

Relationship of the Van Allen radiation belts to solar wind drivers

Journal of Atmospheric and Solar-Terrestrial Physics 70 (2008) 708–729

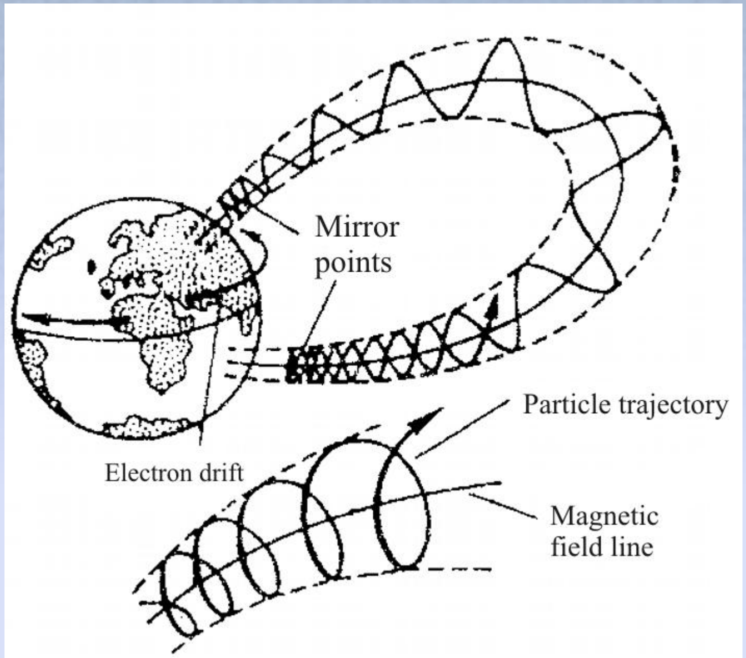

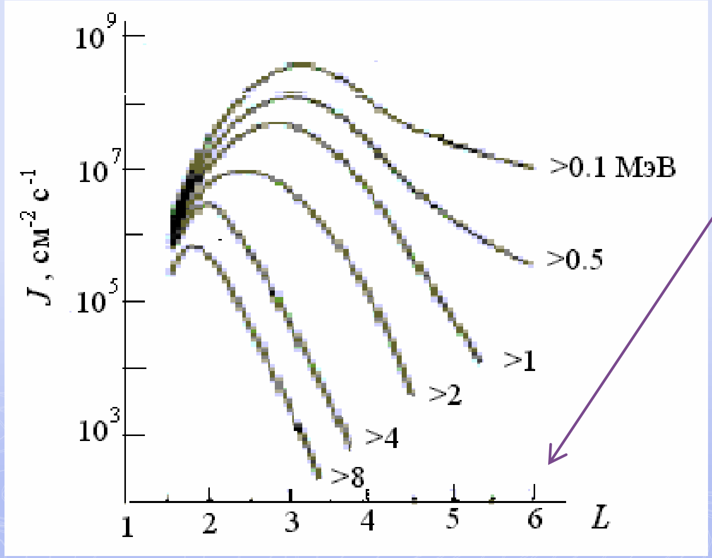

Trajectories of trapped particles have a form of spiral, turns of which are compressed and go to each other with increasing of local filed induction .

At large value of magnetic induction particles are reflected back to equatorial plane.

Trapped particle are reflected at high altitudes (>1000 km)

Quasi – trapped particles are reflected at heights ~ several hundreds km;

Precipitating particles have local mirror points at h~ tens km, or even under ground.

Motion:

1. Rotation around magnetic field line;
2. Oscillation between mirror points in Northern and Southern hemispheres
3. Drift along magnetic latitudes: electrons – to the East, and protons – to the West

L-shell – parameter of drift shell; distance of from the top of field magnetic line to the center of the Earth in the value if Earth radii

Averaged radial profiles of integral omnidirectional proton fluxes

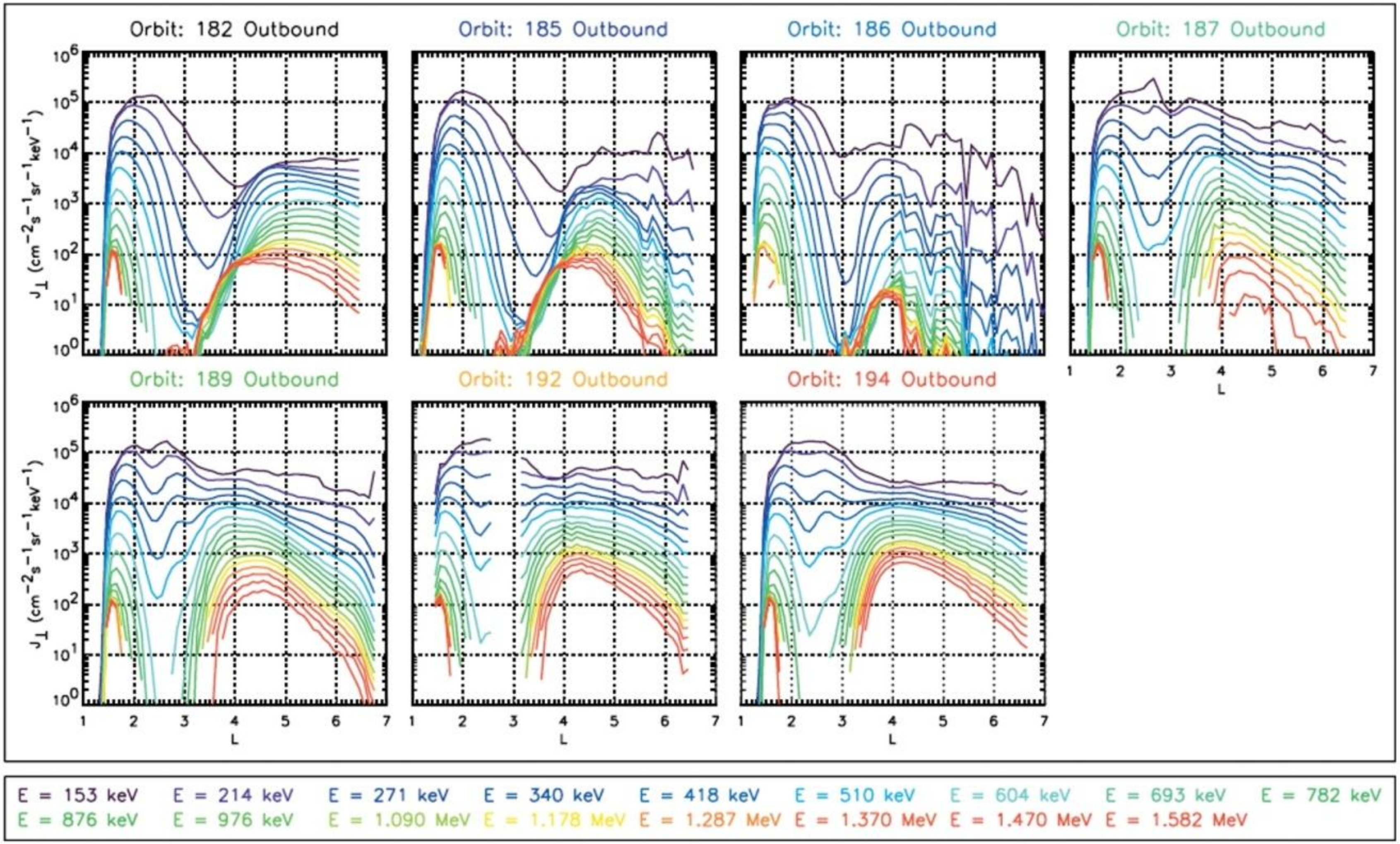

Radial profile of electron flux measured by CRRES satellite at energies from 153 keV to 1.58 MeV showing the two-zone structure of the radiation belts, and variability during geomagnetic storms. Orbits shown here are for prestorm (182), main phase onset (185), minimum Dst (186), and recovery phase (187–194).

R.M. Millan, R.M. Thorne Review of radiation belt relativistic electron losses Journal of Atmospheric and Solar-Terrestrial Physics 69 (2007) 362–377

Richard Horne. Acceleration of killer electrons. *Nature. Physics. Vol.3. September 2007, P. 590-591*

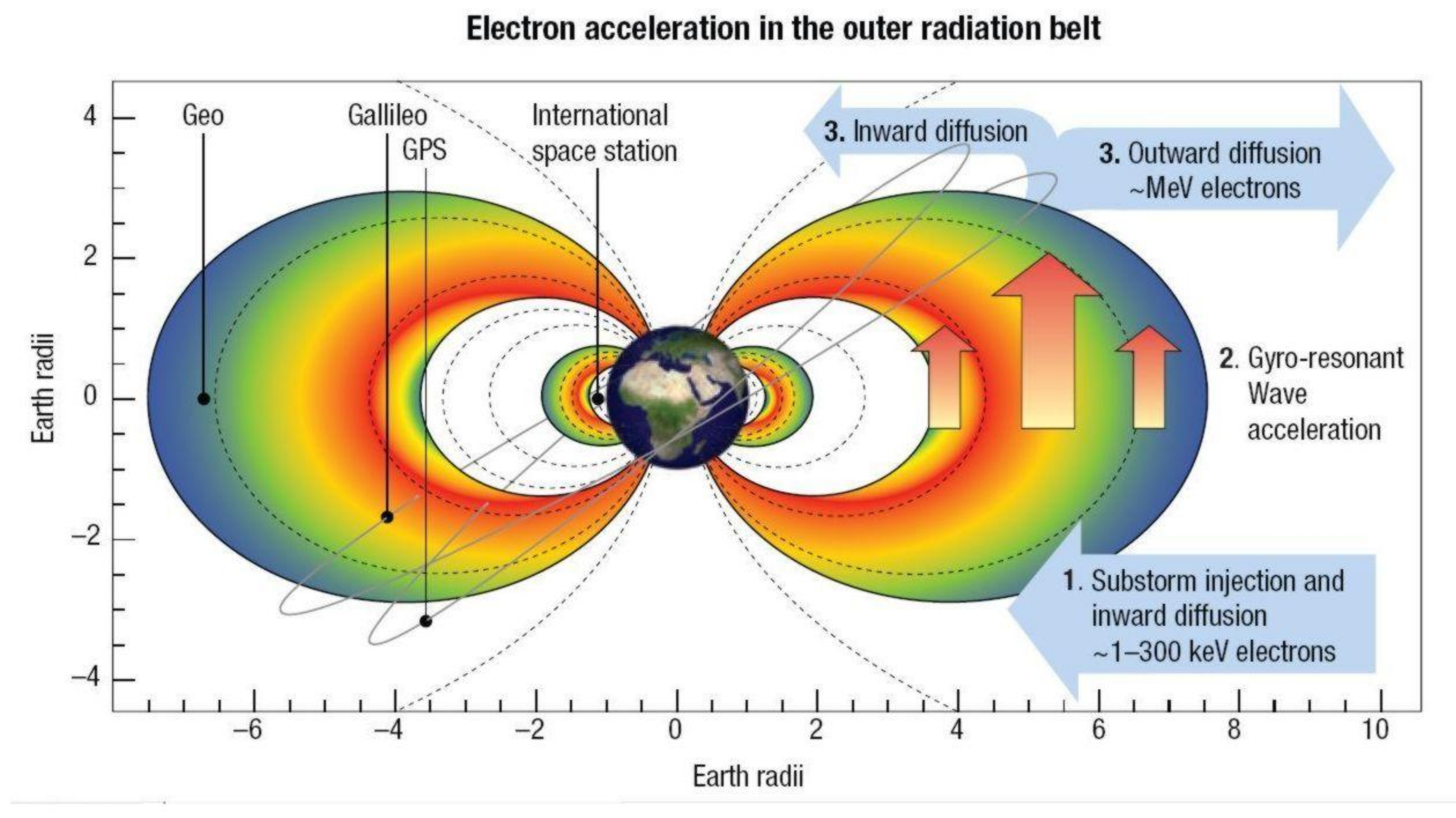

electrons protons

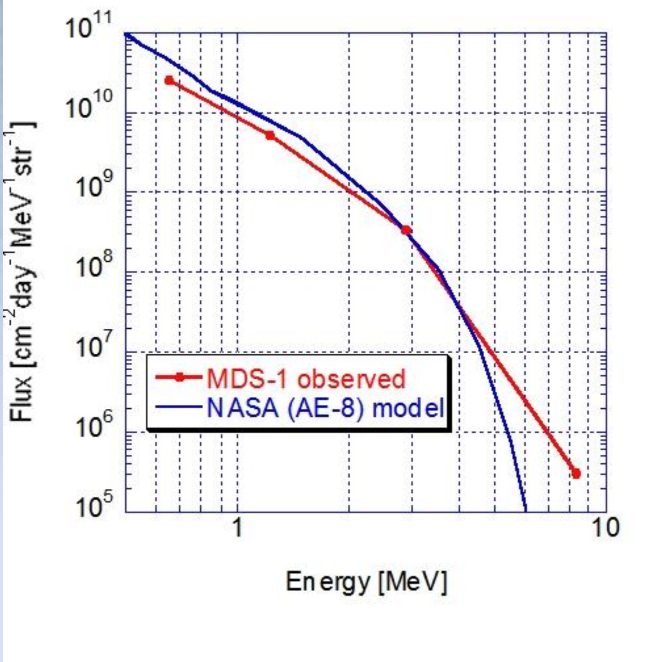

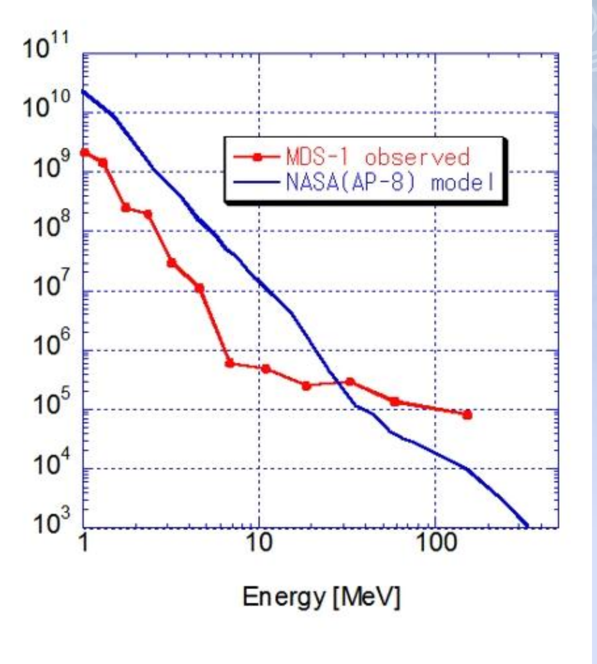

T.Goka, H. Matsumoto, H.Koshiishi, D.Sasada, T. Omodaka
A new empirical Solar-maximum radiation belts model based on measurements of a GTO satellite (Tsubasa),
35th COSPAR Assembly, Paris, PSRB1/F2.9-0005-04

Electron and proton energy spectra averaged by the data of Tsubasa (MDS-1) Japanese satellite in comparison with NASA AE-8 and AP-8 model

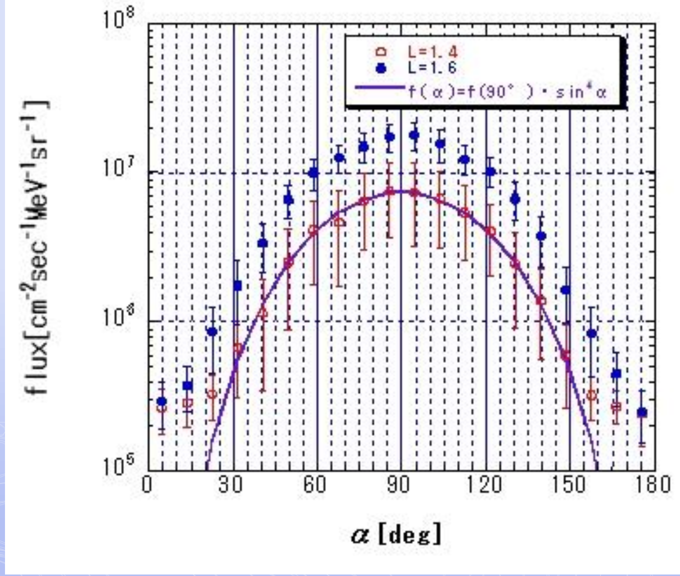

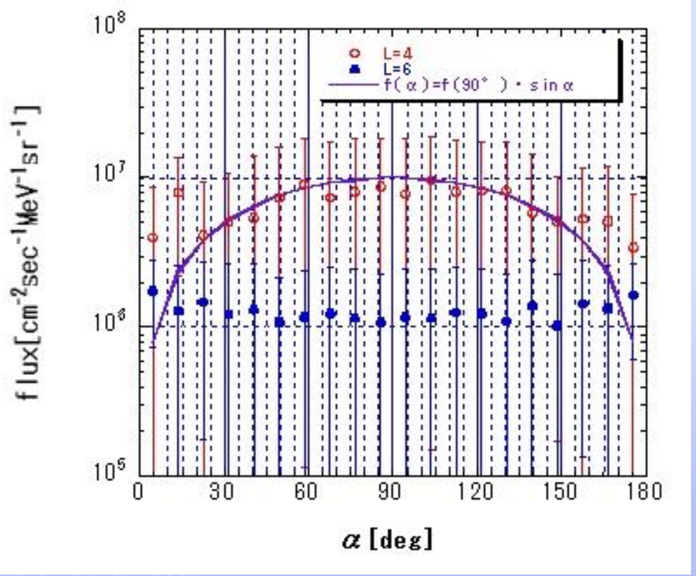

Pitch angle distribution of electrons on geomagnetic equator in the inner belts, on L=1.4, and on L=1.6 (left picture) ,
and in the outer belt on L=4, and on L=6 (right picture)

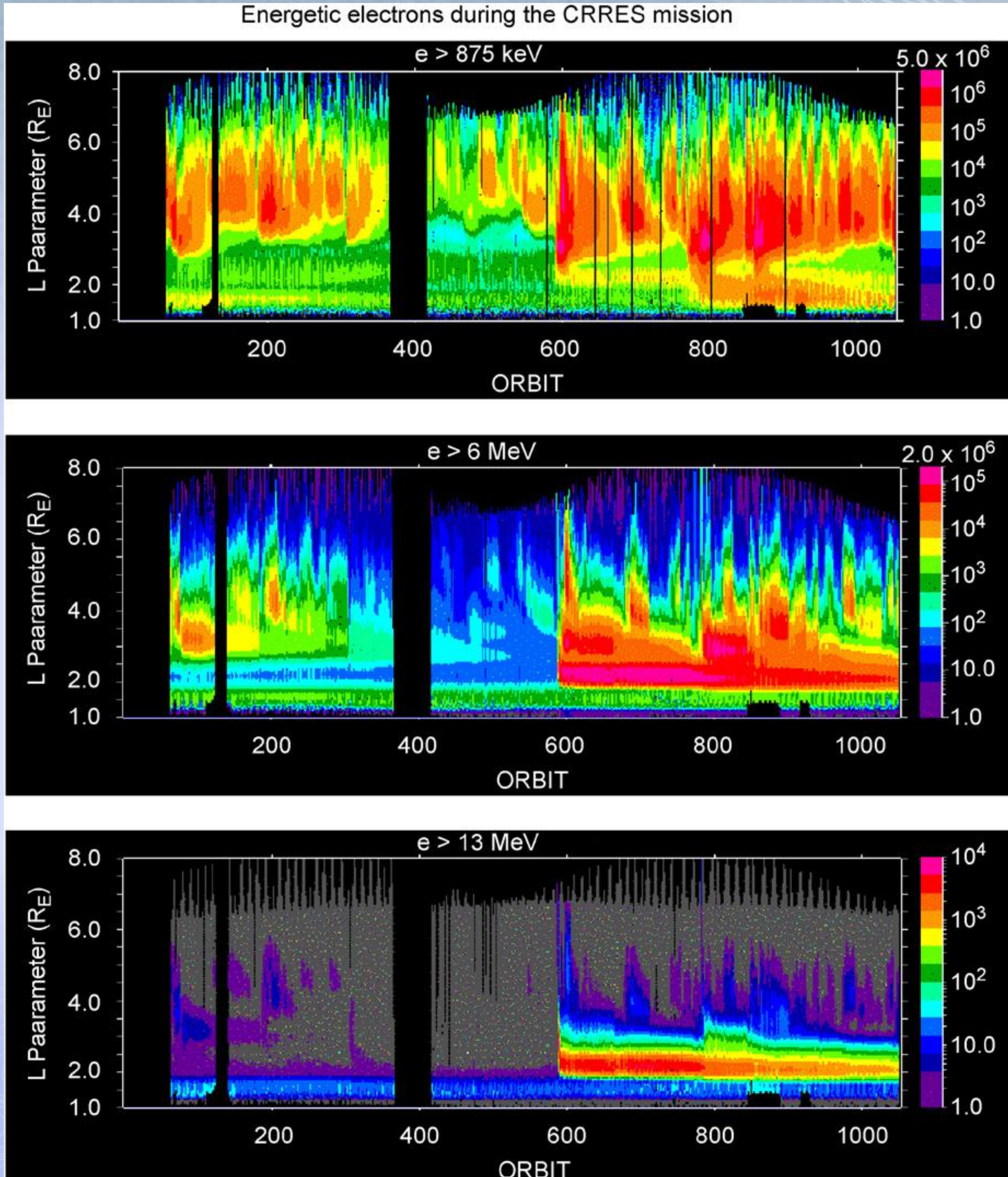

Mary K. Hudson,, Brian T. Kress, Hans-R. Mueller, Jordan A. Zastrow, J. Bernard Blake

Relationship of the Van Allen radiation belts to solar wind drivers

Journal of Atmospheric and Solar-Terrestrial Physics 70 (2008) 708–729

July 1990- October 1991

An event of 24th March 1991 Dst=-300 nT

Integral electron flux levels measured by CRRES over its 14-month lifetime from July 1990 to October 1991 (>0.875, >6 and >13MeV channels). The March 24, 1991 CME-shock injection event is evident as a dramatic change at high energies, filling the electron slot region with ultra-relativistic electrons which persisted for years, as seen by SAMPEX, launched in July 1992

Methods of investigations: instruments, approaches

SC	Year	Altitude, km	Inclination of orbit, deg	Type of detectors	Energies of charged particles
Cosmos 900	1977–1979	500	83	SCD 500 μm	Ee = 30–210 keV
NOAA TIROSN	1978	800	98.9	SCD 700 μm	Ee > 30, >100, >300 keV
Active	1989–1992	500–2500	81.3	SCD 300 μm	Ee = 30–500 keV
OS Mir	1991	400	51.6	Scintillator	Ee > 100, >500, >1500 keV
				Geiger counters	Ee > 75, >300, >600 keV
Coronas-I	1994	500	83	Scintillator	Ee > 0.5 MэB
SAMPEX	1992–1998	520–670	82	SCD telescope	Ee > 150 keV
OS Mir	1999	350	51.6	SCD 300 μm	Ee = 0.3–1.5 MэB
CoronasF	2001–2005	500	82.5	SCD telescope	Ee = 0.3–12 MэB
NOAA POES15	1998	800	98.9	SCD 700 μm	Ee > 30, >100, >300 keV
NOAA POES16	2001	"	"	"	"
NOAA POES17	2002 "	"	"	"	"
NOAA POES18	2005 "	"	"	"	'
SERVIS	2003–2005	980–1020	99.5	SCD + scintillator	Ee = 0.3–10 MэB
Universitetsky–Tat'yana	2005–2007	920–980	83	SCD 300 μm	Ee > 70 keV
				SCD 1 mm	Ee = 300–900 keV

V. A. Sadovnichy, *M. I. Panasyuk, I. V. Yashin, V.O. Barinova, N. N. Veden'kin, N. A. Vlasova et al.*

Investigations of the Space Environment Aboard the *Universitetsky–Tat'yana and Universitetsky–Tat'yana2* Microsatellites

Solar System Research, 2011, Vol. 45, No. 1, pp. 3–29

Methods of investigations: instruments, approaches

Outside of the magnetosphere

Advanced Composition Explorer (ACE)

The Solar Energetic Particle Ionic Charge Analyzer (SEPICA)

Energy Range	Elements
H: 0.2 - 3 MeV	
He: 0.3 - 6 MeV/N	H to He
O: 0.2 - 15 MeV/N	H to O
Fe: 0.1 - 5.4 MeV/N	O to Fe

Resource	Measured
mass	37.4 kg
Power	18.5 W nominal, 19.5 W peak
average data rate	608 bps

Main detectors: 1) multi-ware dE/dx proportional counter, 2) Ion-implanted silicon pixel detectors of 500 μm thickness, 3) anticoincidence detector – CsI(Tl) scintillator

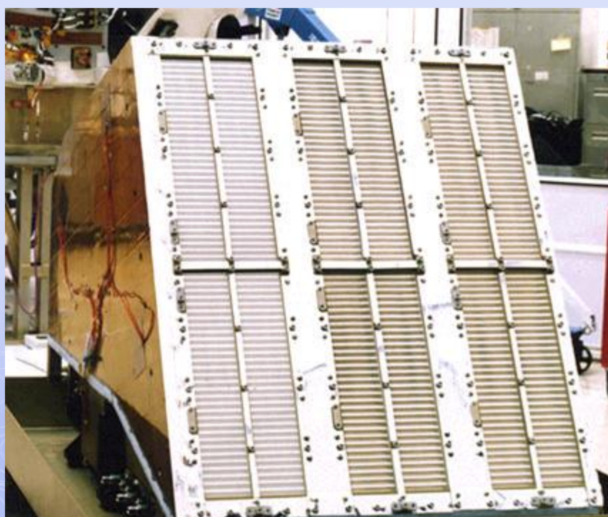

STEREO Ahead and STEREO Behind

SEP (Solar Energetic Particle) is made up from the Suprathermal Ion Telescope (SIT), the Solar Electron and Proton Telescope (SEPT), the Low Energy Telescope (LET) and the High Energy Telescope (HET) . Totally:

Electrons: 0.03-6 MeV,
Protons: 0.06-100 MeV
Helium: 0.12-100 MeV/nuc
>Helium 0.03-49 Mev/nucl

SEP:	Mass	Power	Data rate
LET	1.32 kg	1.18 W	577 bps
HET	0.60 kg	0.36 W	218 bps
SEP centr	2.19 kg	4.06 W	9 bps
SIT	1.63 kg	1.65 W	424 bps
SEPT-E	0.80 kg	0.60 W	40 bpsg
SEPT-NS	1.18 kgf	0.60 W	40 bpsg

Main detectors: 1) ion-implanted planar silicon detectors, 2) solid-state detectors

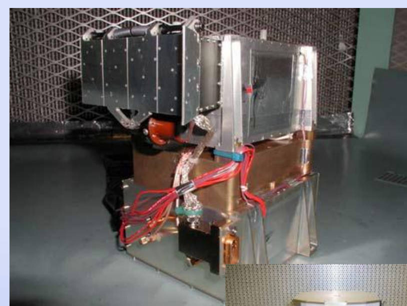

NOAA GEOSTATIONARY ORBIT SATELLITES

GOES-8 , GOES9, GOES10, GOES11, GOES12

The Energetic Particle Sensor (EPS) and the High Energy Protons and Alpha Detector (HEPAD)

EPS – Telescope and Dome: silicon surface barrier solid State detectors: 50 μm, 100 μm, 500 μm and S=200 mm**2

		Primary Detector Response		Secondary Detector Response	
Proton Channels	Detector Type	Energy Range (MeV)	Channel Response Factor† (cm^2 sr MeV)	Energy Range (MeV)	Geometric Factor (cm^2 sr)
P1	Telescope	0.7–4.2	0.194	50–200	0.02
P2	Telescope	4.2–8.7	0.252	50–125	0.04
				125–200	0.007
P3	Telescope	8.7–14.5	0.325	60–125	0.07
				125–200	0.014
P4	Dome 3	15–40	5.21	80–115	0.038
				115–150	0.25
P5	Dome 4	38–82	14.5	80–110	0.091
				110–150	0.57
				150–190	0.21
P6	Dome 5	84–200	129.	80–110	0.15
				110–130	0.84
				130–200	0.80
				200–300	0.26
P7	Dome 5	110–900	839.	80–110	0.03
				110–170	0.15
				170–250	1.5
				250–500	1.9
				500–900	0.56
P8	HEPAD	330–420	65.7		
P9	HEPAD	420–510	65.7		
P10	HEPAD	510–700	139.		
P11	HEPAD	> 700	G = 0.73 cm^2 sr		
Electron Channels					
E1	Dome 3	> 0.6	Spectrum Dependent (see text)		
E2	Dome 3	> 2	0.05		
E2	Dome 4	> 4	Spectrum Dependent (see text)		
Alpha Channels					
A1	Telescope	4–10	0.342		
A2	Telescope	10–21	0.638		
A3	Telescope	21–61	2.22		
A4	Dome 3	60–160	21.		
A5	Dome 4	160–260	36.		
A6	Dome 5	330–500	176.		
A7	HEPAD	2560–3400	613.		
A8	HEPAD	> 3400	G = 0.73 cm^2 sr		
Derived Proton Integral Flux Values					
		> 1			
		> 5			
		> 10			
		> 30			
		> 50			
		> 60			
		> 100			

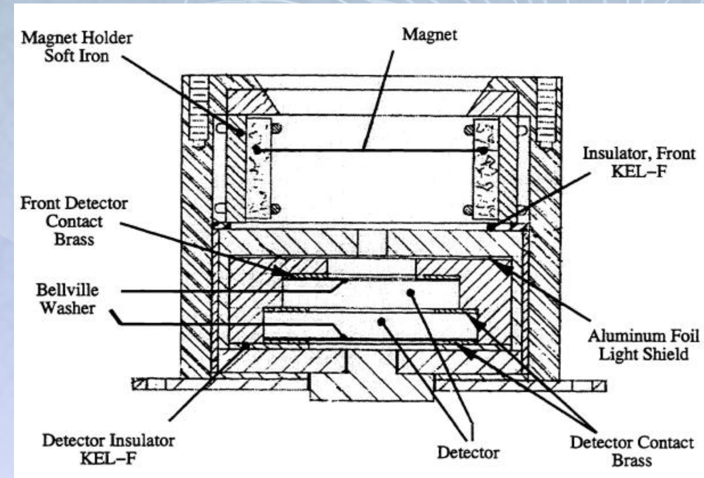

Mass: 15kg;
Power: 20 Watts

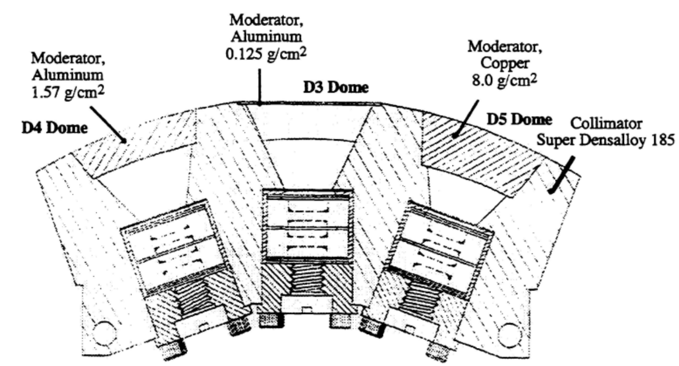

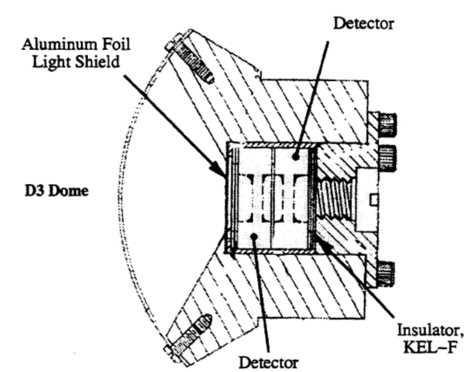

BepiColombo ESA mission to Mercury (2015)

Solar Intensity X-ray and particle Spectrometer (SIXS)

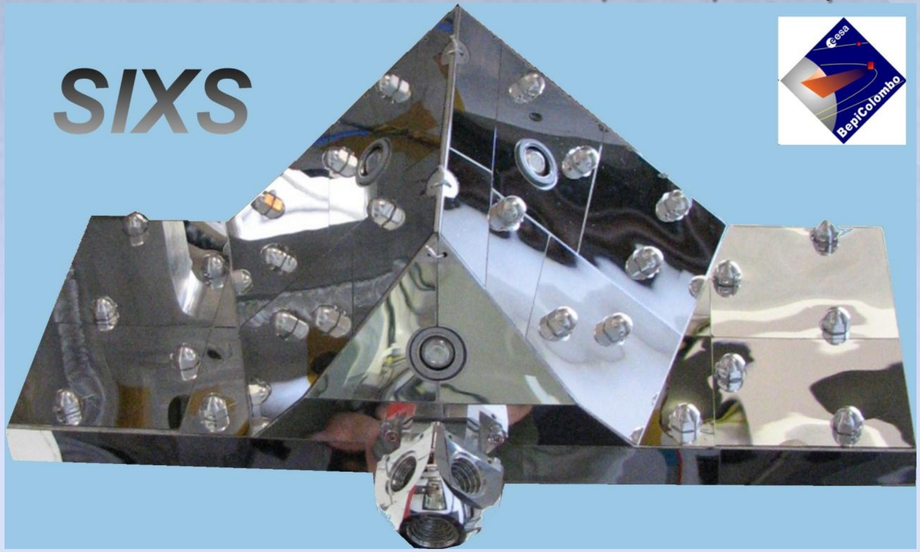

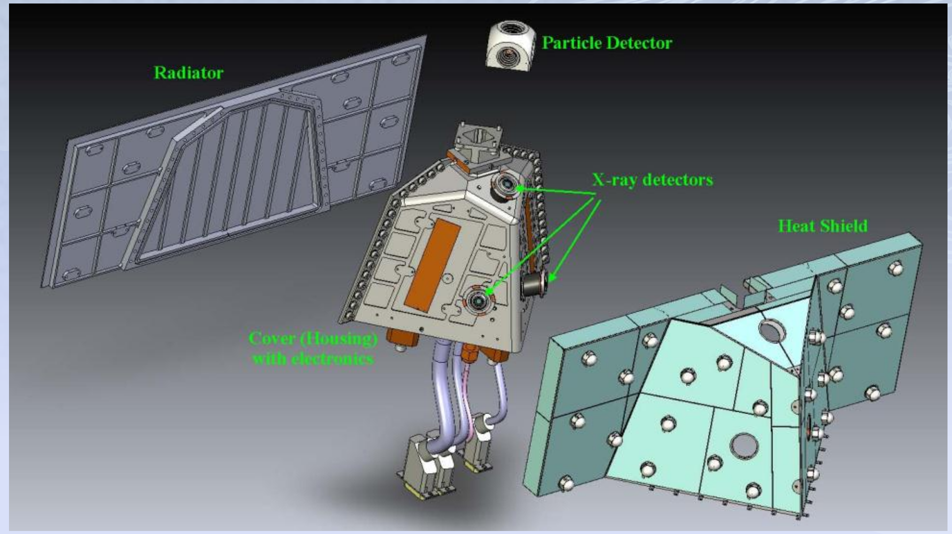

Credit: Juhani Huovelin, PI of the SIXS instrument, University of Helsinki (Finland)

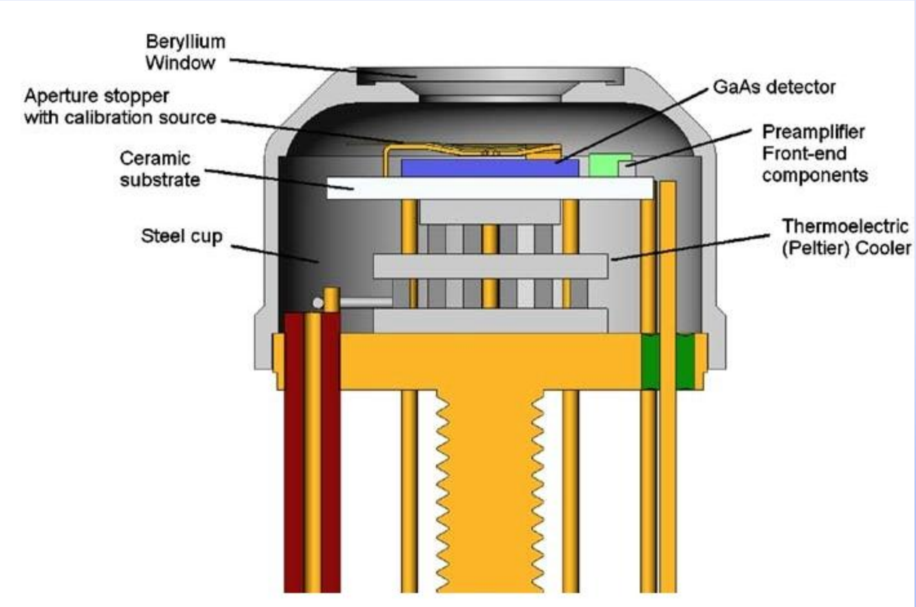

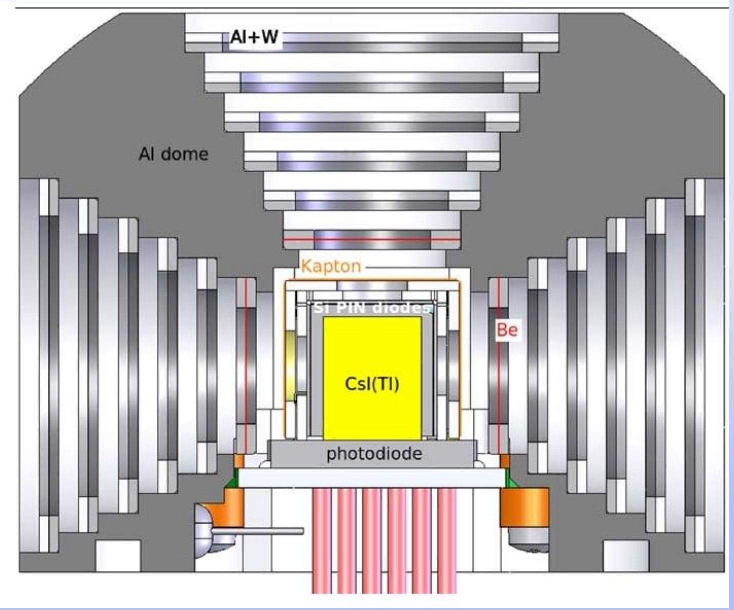

The **S**atellite **T**elescope of **E**lectrons and **P**rotons **STEP-F** and the **S**olar **ph**otometer **in X**-rays **SphinX** aboard the «CORONAS-Photon“ spacecraft

SphinX

STEP-F

SphinX

STEP-F

Z

Technical parameters of the STEP-F device

- Mass:
  STEP-FD — 15.4 kg;
  STEP-FE — 2.7 kg;
- Power consumption:
  STEP-FD — 40 Watt;
  STEP-FE — 8 Watt;
- Dimensions:
  1) STEP-FD:
  337 mm x 395 mm x 293 mm;
  2) STEP-FE:
  95 mm x 287 mm x 160 mm;
- Full angle of view:
  — 108 x 108° for lowest energies;
  — 98 x 98° for highest energies

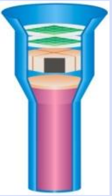

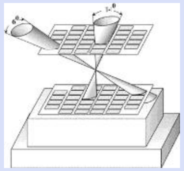

- Active areas:
  semiconductor detectors – 20 cm^2;
  scintillation detectors – 36 и 49 cm^2;
- Geometry factors:
  from 21.7 cm^2 • sr for low energies of particles,
  to 12.4 cm^2 • sr for high energies of particles
- Temporal resolution:
  2 seconds — 12 values in each half of minutes;
  30 seconds — 1 value in each first 24 seconds of each half of minutes
  (*6 seconds is transmission of information*)

- Energy ranges:
  Electrons:
  1) 0.35 – 0.95 MeV;
  2) 1.2 – 2.3 MeV;
  3) > 2.3 MeV
- Protons:
  1) 7.4 – 10.0 MeV;
  2) 15.6 – 17.5 MeV;
  3) 17.5 – 19.6 MeV;
  4) 19.6 – 22.2 MeV;
  5) 22.2 – 25.4 MeV;
  6) 25.4 – 29.3 MeV;
  7) 29.3 – 33.2 MeV;
  8) 33.2 – 38.9 MeV;
  9) 38.9 – 46.5 MeV;
  10) 46.5 – 55.2 MeV;
  11) > 55.2 MeV

Channels of mixed particle registration:
1) e (E_e=0.18-0.51 MeV) + p (E_p=3.5-3.7 MeV)
2) p (E_p=3.7-7.4 MeV) +e (E_e=0.55-0.95 MeV);
3) α ($E_α$ =15.9-29.8 MeV) + p (E_p=7.4-10.0 MeV);

Basic parameters of SphinX detector measurement channels

Detector	D1	D2	D3	D4
Aperture, mm_2	21.500 A	0.4947 S	0.01008 S	11.1 A
Energy FWHM, eV	480 B	350 B	370 B	290 P
Shaping time FWHM, μs	1.25 e	4.17 e	4.17 e	4.17 e

Notes: A—based on Amptek technical drawings of respective detector, S—measured at SCR Wroclaw under microscope, B—based on BESSY measurements, P—based on Palermo XACT measurements, e—estimated value.

S. Gburek, J. Sylwester, M. Kowalinski, J. Bakala, Z. Kordylewski, P. Podgorski, S. Plocieniak, M. Siarkowski, B. Sylwester, W. Trzebinski, S. V. et al. *SphinX Soft X-ray Spectrophotometer: Science Objectives, Design and Performance. Solar System Research, 2011, Vol.**45**, No. 3, p.189-199.*

Radiation maps of the Earth in different energy channels from STEP-F device measurements

The averages have been calculated from measurements covering the period between March, 3 and April, 1, 2009

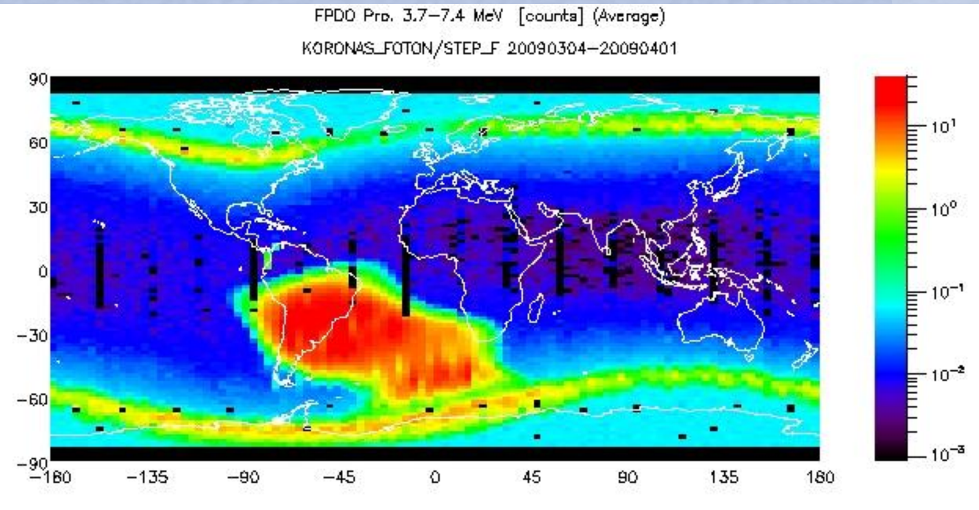

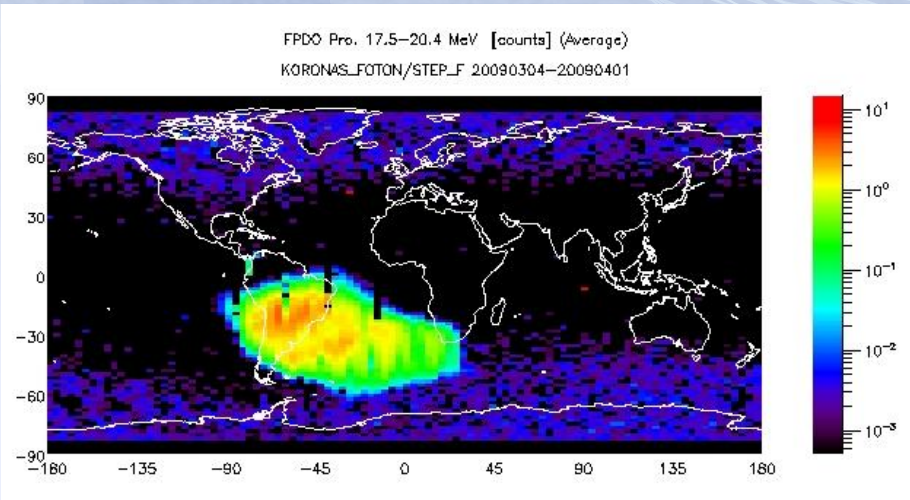

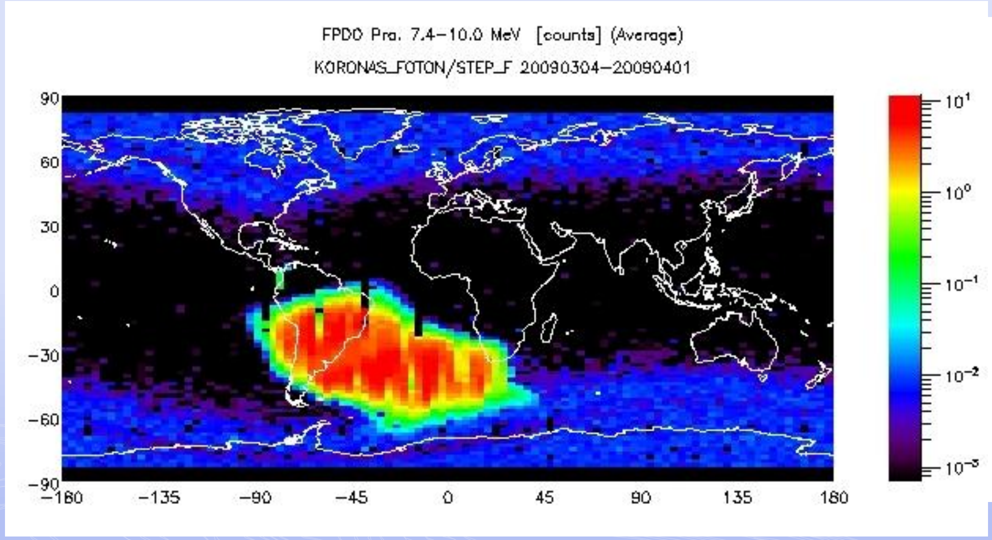

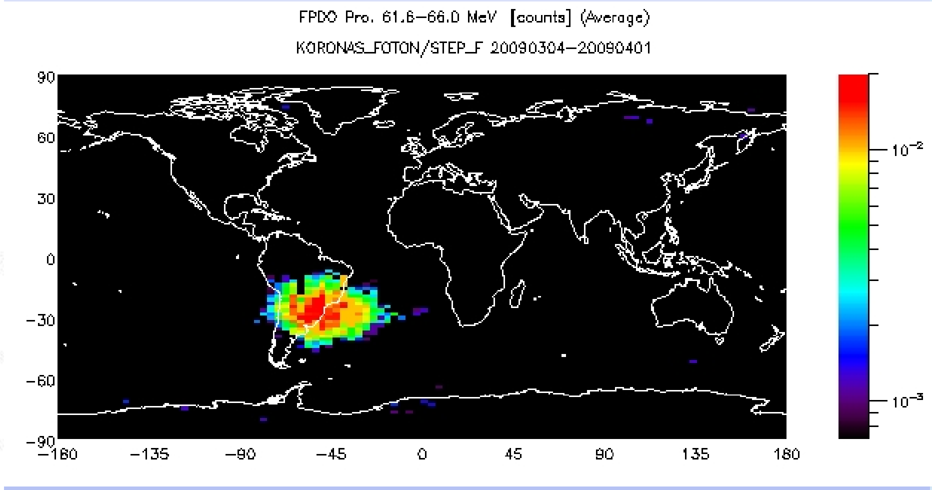

In the last of 256 SphinX energy channels there were collected particle related signals, which corresponds to the energies above 15 keV. It can be found that count rate in the last channel was significantly increased when spacecraft crossed through the South Atlantic Anomaly and Radiation Belts. This characteristic pattern was seen in data from both Det1 and Det2 SphinX detectors Figure below shows that SphinX is able to take measurements of Earth's particle environment. The averages have been calculated from measurements covering the period between March and October 2009

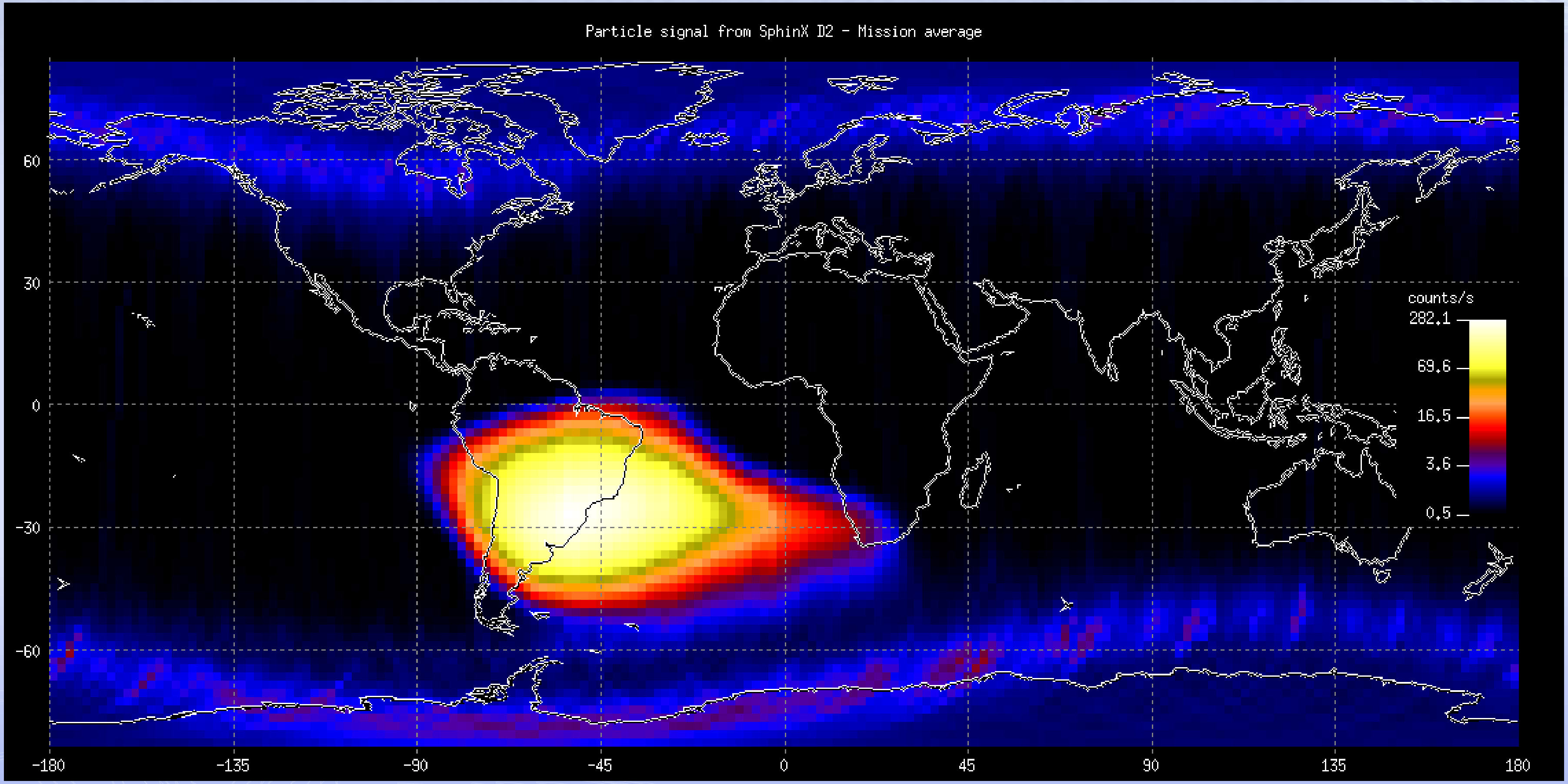

Typical initial temporal variations of electron fluxes of intermediate energies in May, 2009 from the data of the STEP-F device. Time resolution: 2 seconds

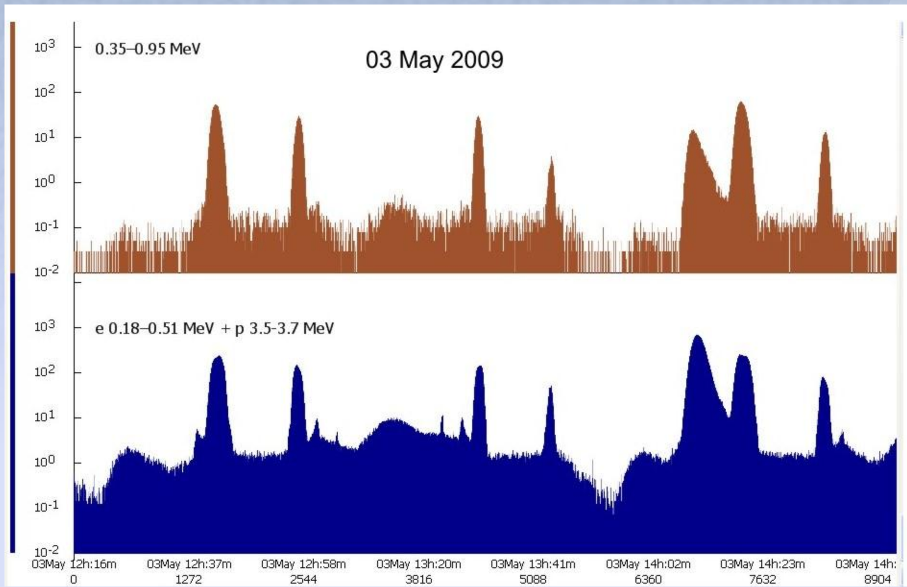

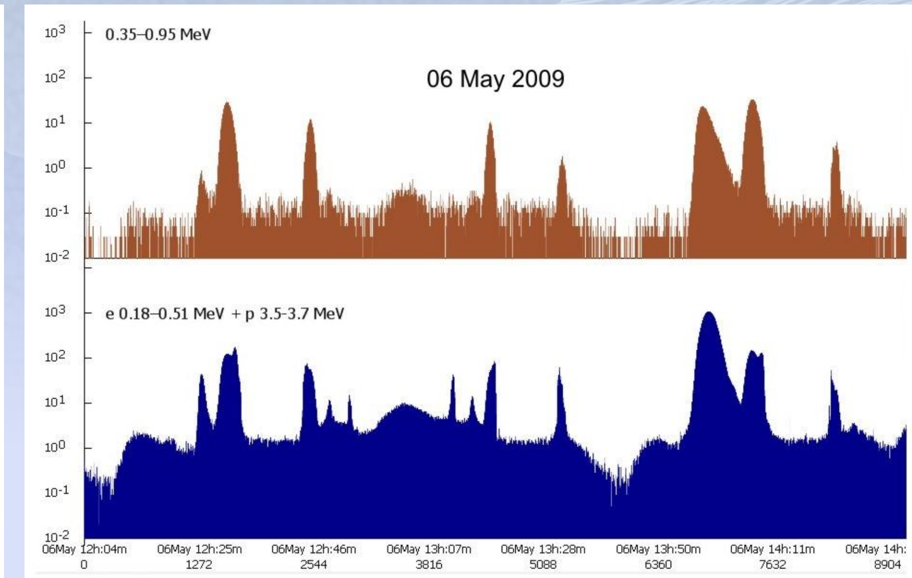

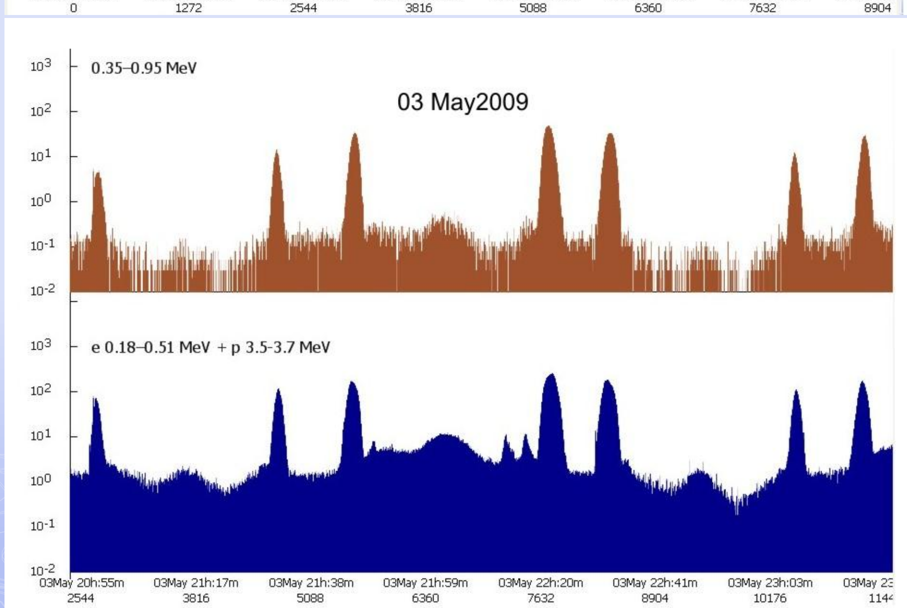

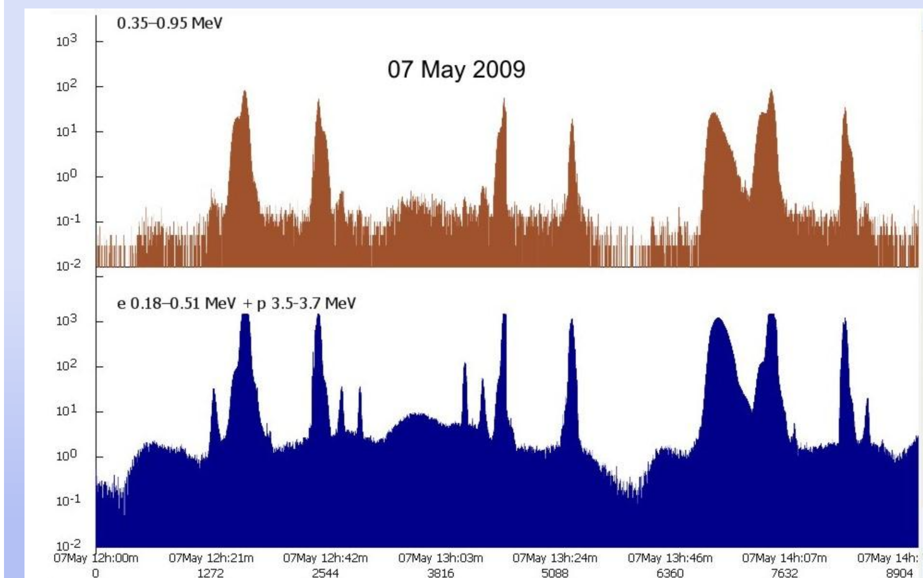

Joint analysis of particle fluxes deviation in May, 2009. Approach 1: temporal rows

May, 8, 2009

Blue – D2e (electrons 0.35-0.95 MeV of STEP-F)
Brown – Det1 of SphinX
Red – Det2 of SphinX, units:
STEP-F – in part./cm^2 s sr; SphinX – in part./cm^2

1. There are integral energy thresholds E_{thr1} and E_{thr2} for registration of electrons by Det1 and Det2 of **SphinX** device.
2. Trend of Det1 (Sphinx) repeat trend of D2e (STEP-F) very well.
3. E_{thr1} is between 0.2 and 0.35 MeV.
4. Sensitivity of Det1 and Det2 (Sphinx) is worse then that one of STEP-F in factor ~100.
5. Sensitivity of Det1 is better then sensitivity of Det2 for SphinX device

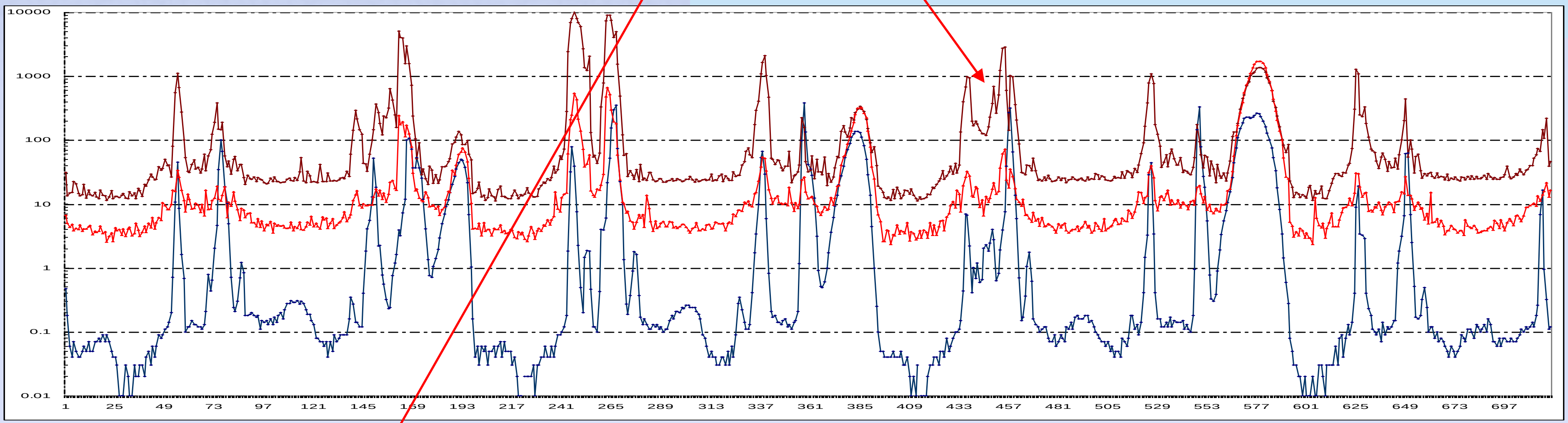

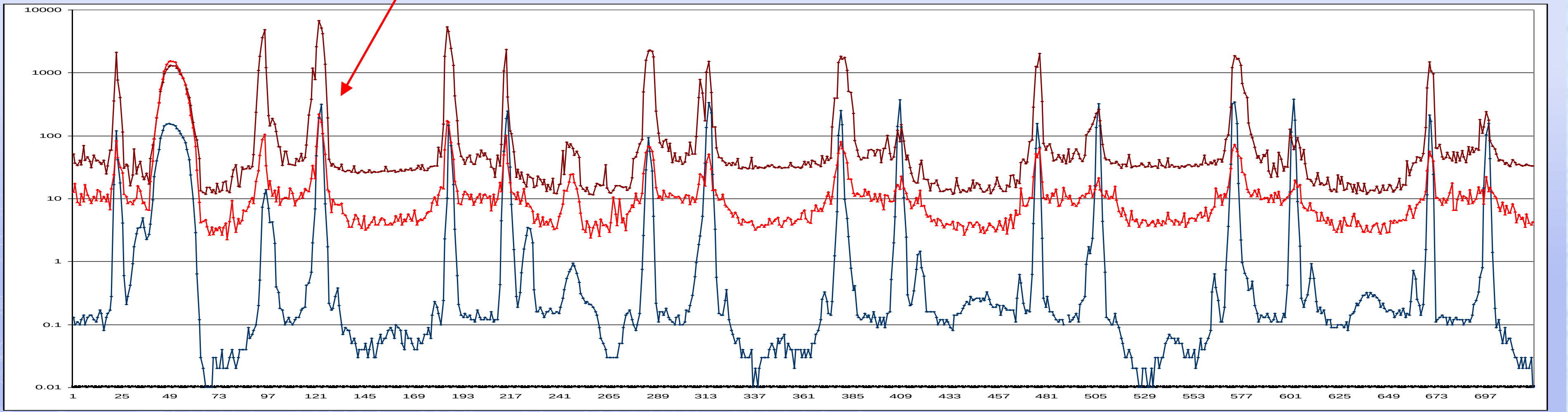

Joint analysis of particle fluxes deviation in May, 2009.

Approach 2: Distribution of particle fluxes inside the South Atlantic Anomaly

Definition of particle energies registered by the SphinX device means definition of integral energy thresholds Ethr

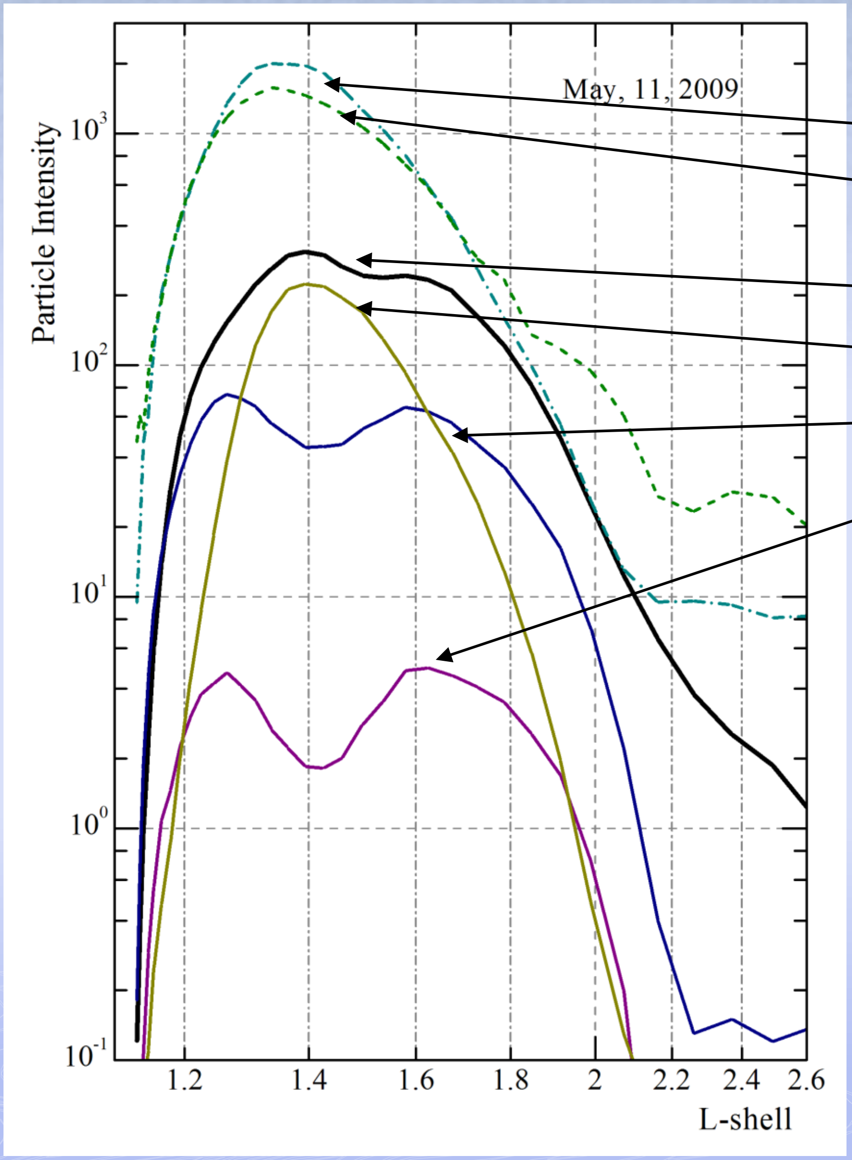

Conclusions:

1. It can be seen 2 maximums in the fluxes from STE-F measurements by direct methods, i.e. electrons. It looks like split of inner belt.
2. Direction of electron flux coincided with fields of view of both devices. But really FoVs of both devices are perpendicular to each other.
3. It means that electron fluxes are isotropic.
4. Profiles of Det1, Det2 (SphinX) and D4e (**STEP-F**) are very close to each other,. Let us do not forget that D4e detects secondary gamma-quanta generated by primary electrons inside CsI(Tl) and construction materials .

Joint analysis of particle fluxes deviation in May, 2009.

Approach 2: Distribution of particle fluxes inside South Atlantic Anomaly *(continuation)*

D2e (STEP-F) 0.35-0.95 MeV	D1p (STEP-F) 0.55-0.95 MeV	Det1 (Sphinx) ?	Det2 (Sphinx) ?	D1a (STEP-F) 0.57-0.95 MeV
1.41	1.32	1.41	1.41	1.32
1.4	1.31	-	-	1.3
1.41	1.3	1.38	1.38	1.3
1.4	1.31	1.37	1.37	1.29
1.39	1,3	1.39	1.39	1.3
1.4	1.29	1.37	1.4	1.29
1.39	1.28	1.385	1.36	1.27
1.4	1.29	1.34	1.4	1.27
1.39	1.28	1.36	1.36	1.26
1,38	1.27	1.35	1.35	1.26
1.39	1.27	1.34	1.34	1.27
1.41	1.27	1.32	1.35	1.25
1.39	1.26	1.33	1.33	1.24
1.38	1.27	1.32	1.32	1.27
1.3957	**1.2871**	**1.3588**	**1.3661**	**1.278**
+-0.010	**+-0.018**	**+-0.028**	**+-0.028**	**+-0.022**

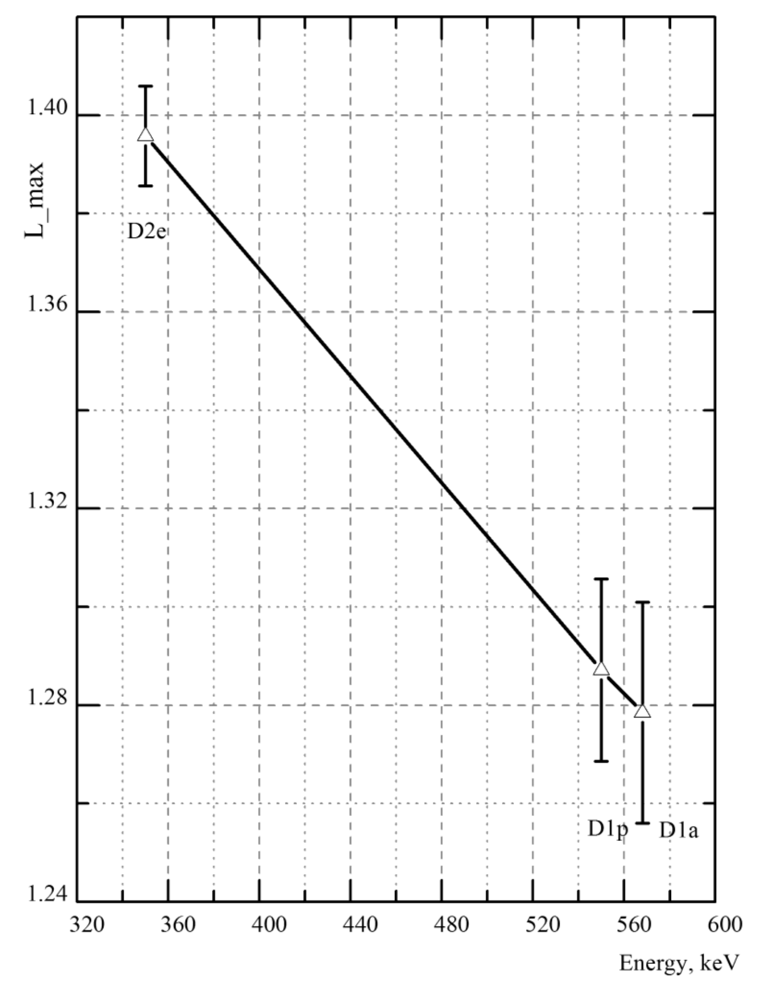

Dependence of L-shell with maximal values of particle intensities as a function of electron energy during 1-14 May, 2009 for the STEP-F device.

Joint analysis of particle fluxes deviation in May, 2009.

Approach 2. Distribution of particle fluxes inside South Atlantic Anomaly *(continuation)*

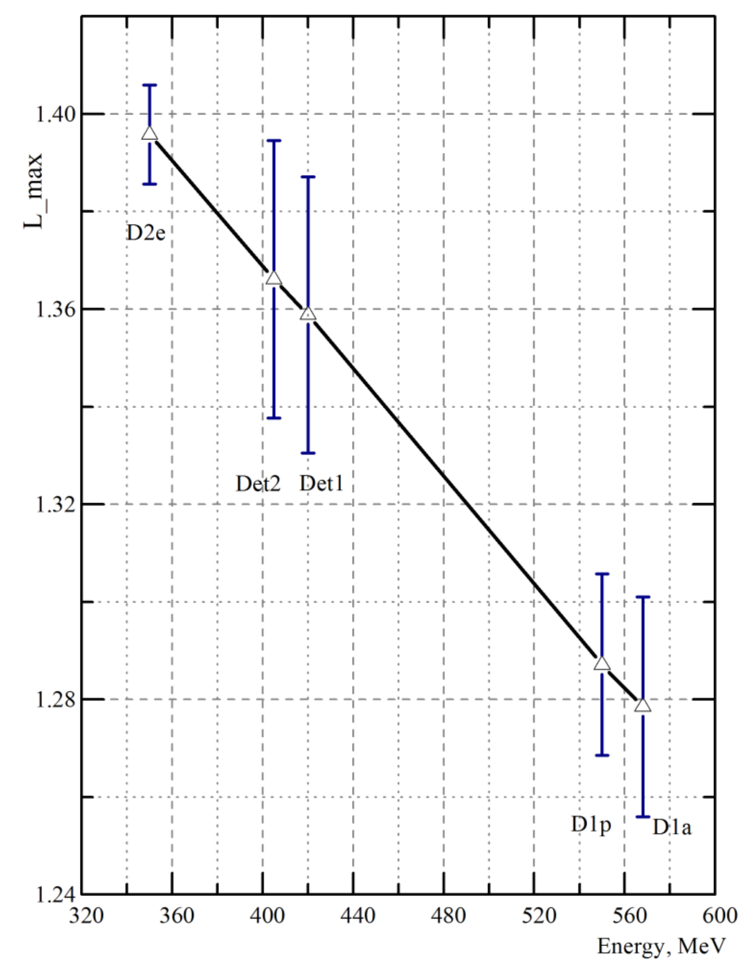

Day E_{thr}, keV	May, 1	May, 8	May, 14
Det1	350	455	460
Det2	350	350	460

1. Variation of L-max for Det1 and Det2 (SphniX) is rather wide
2. There are different values of threshold energies of Det1 and Det2 at various days of May, 2009.
3. Suggestion is: that effective energy of electron registration for Det1 and Det2 is changed from day to day. It may be if the energy spectrum is changed too, and spectra of secondary quanta are changed.

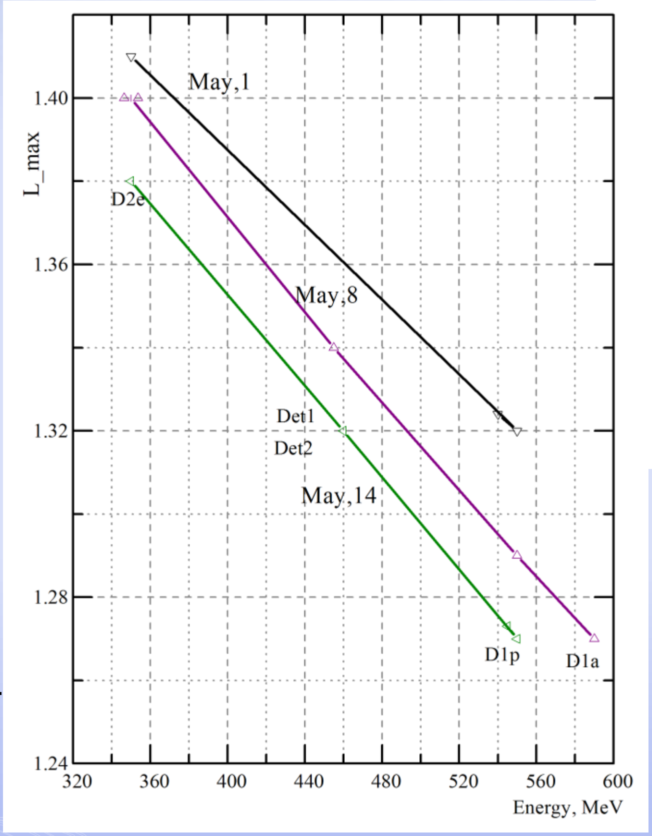

The same distribution, but jointly with values of L-max for Det1 and Det2 (SphinX). From the curve we can find that

E_{thr1}=420 keV, and **E_{thr2}=405 keV**

Joint analysis of particle flux variations in May, 2009.

Approach 3. Distribution of particle fluxes in Radiation Belts

Definition of particle energies registered by the SphinX device in Radiation Belts

Two approaches can be applied:
1. Distribution of maximal spectral flux densities on L-shells (like in case of SAA);
2. Distribution of ΔL on the particle energy during radial diffusion in time the weak geomagnetic storm.

Radial and pitch-angle diffusion of electrons by D2e channel of the ***STEP-F*** *device*

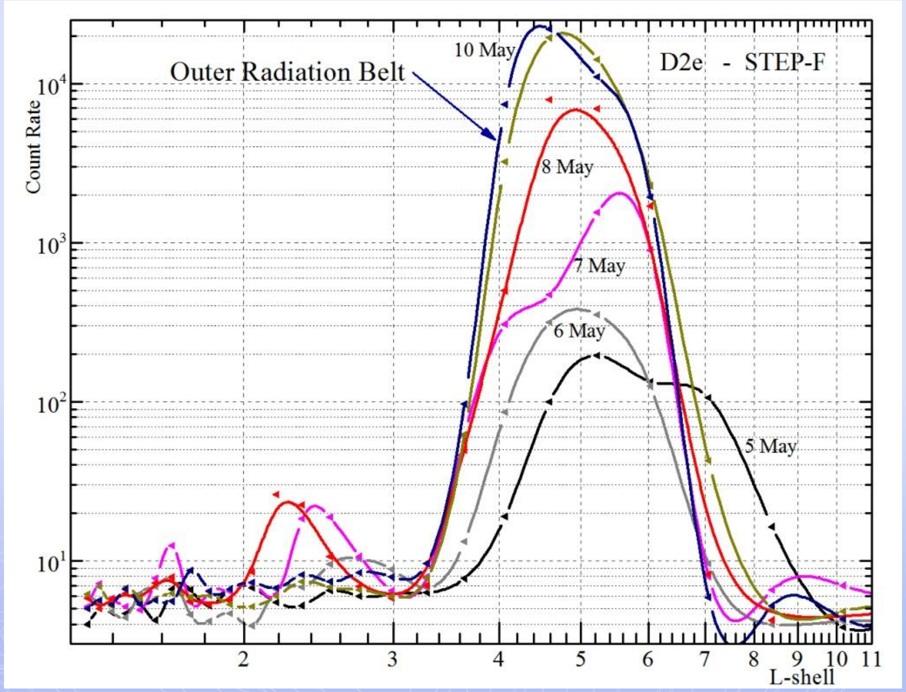

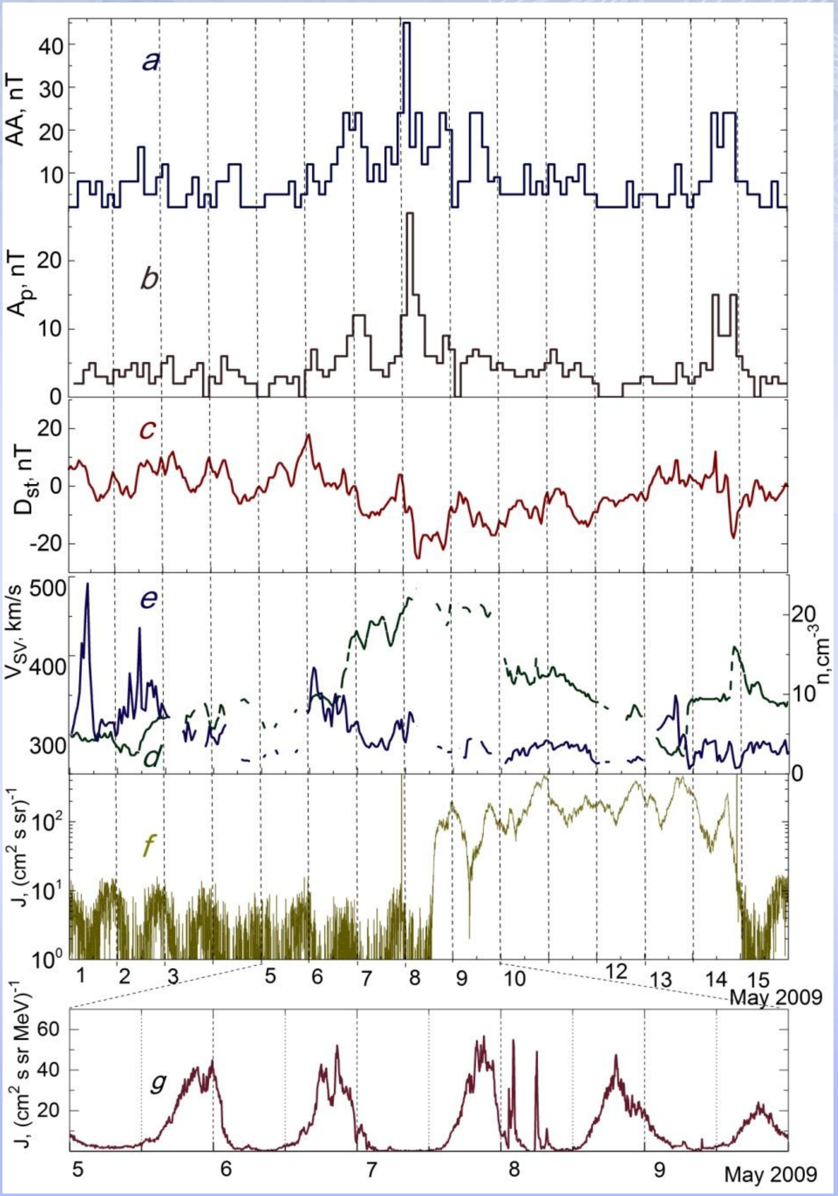

Joint analysis of particle flux variations in May, 2009.

Approach 3. Distribution of particle fluxes in Radiation Belts *continuation*

Radial and pitch-angle diffusion of electrons by Det1 and Det2 detectors of the SphinX device

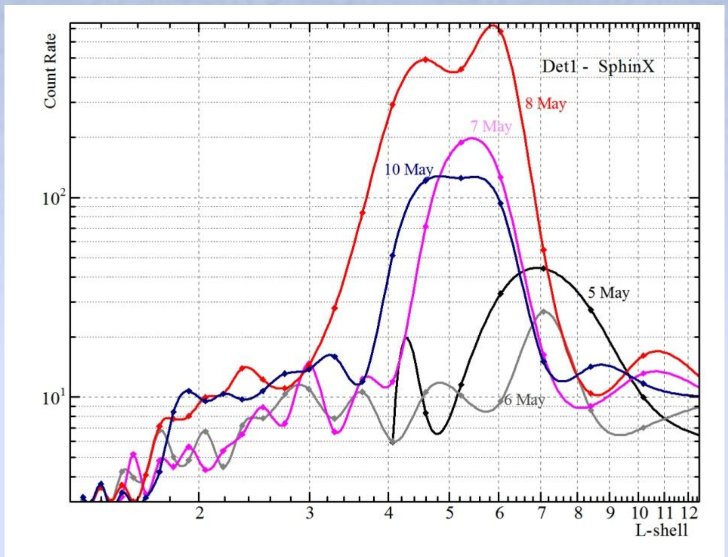

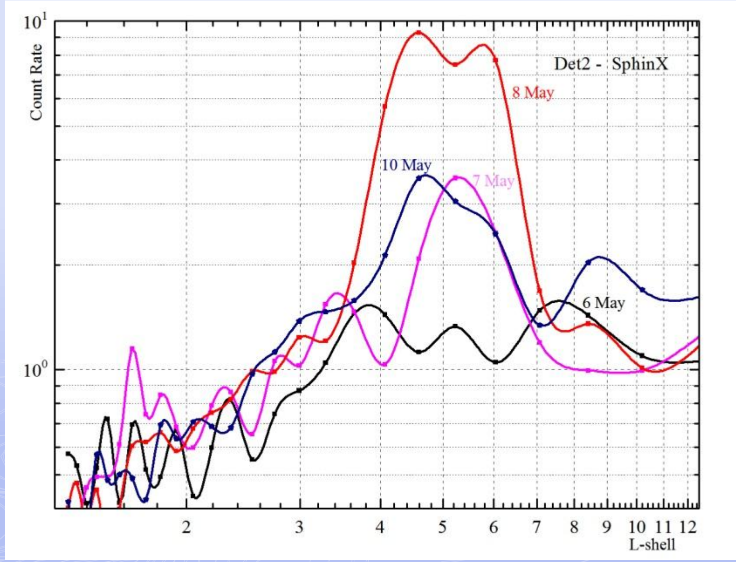

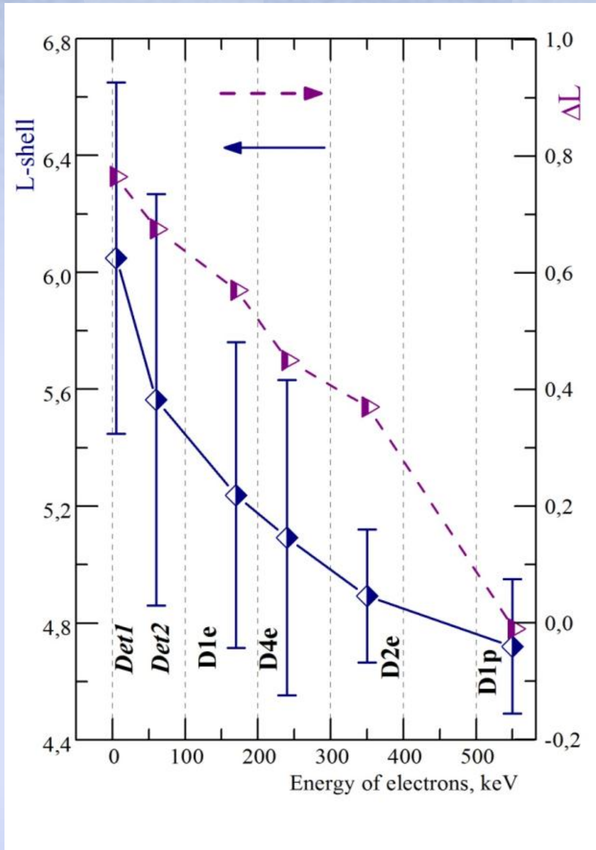

For the Earth's outer radiation belt effective values for electron recording by the SphinX device were, respectively, **Ethr1 ≈ 5 keV, Ethr2 ≈60 keV.** These values are not strictly fixed. They are functions of the spatial position of the sensors in a particular area of charged radiation, whether in its center or at the periphery, as well as of the level of geomagnetic disturbance.

So, the main species registered by Det1 and Det2 detectors of the SphinX device in last energy channel of spectrometer is secondary gamma-quanta generated in shielding of the TESIS instrument and collimator of the SphinX device.

Anisotropic fluxes of electrons at the altitudes ~550 km , 13th orbit, descending node

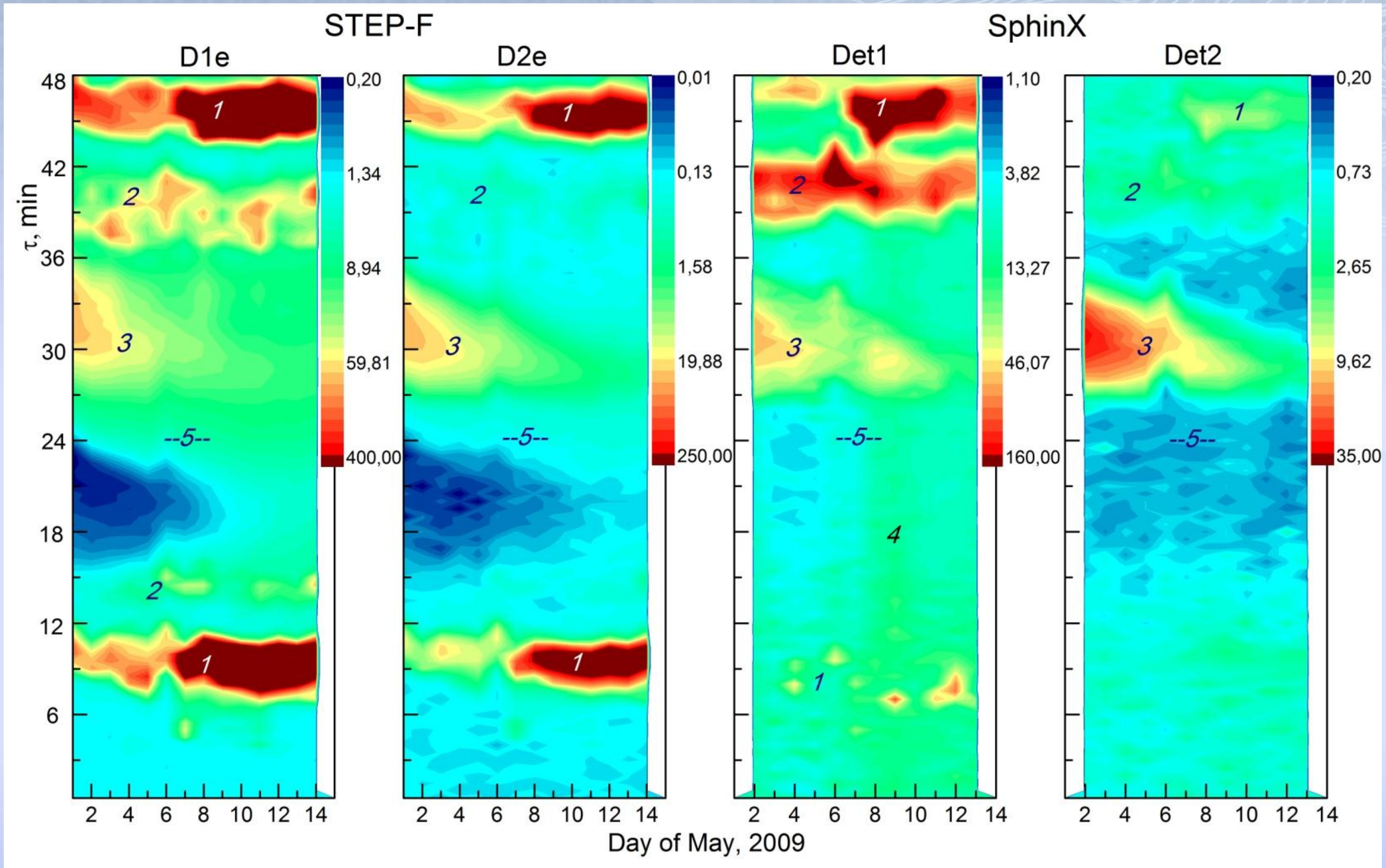

1 - outer belt, 2- inner belt, 3 - zone of enlarged particle fluxes on L=1.1-1.4 , 4 - precipitating particles during the main phase of geomagnetic storm registered by Det1 of SphinX, 5 - geographic equator zone

Some selected results from the STEP-F device

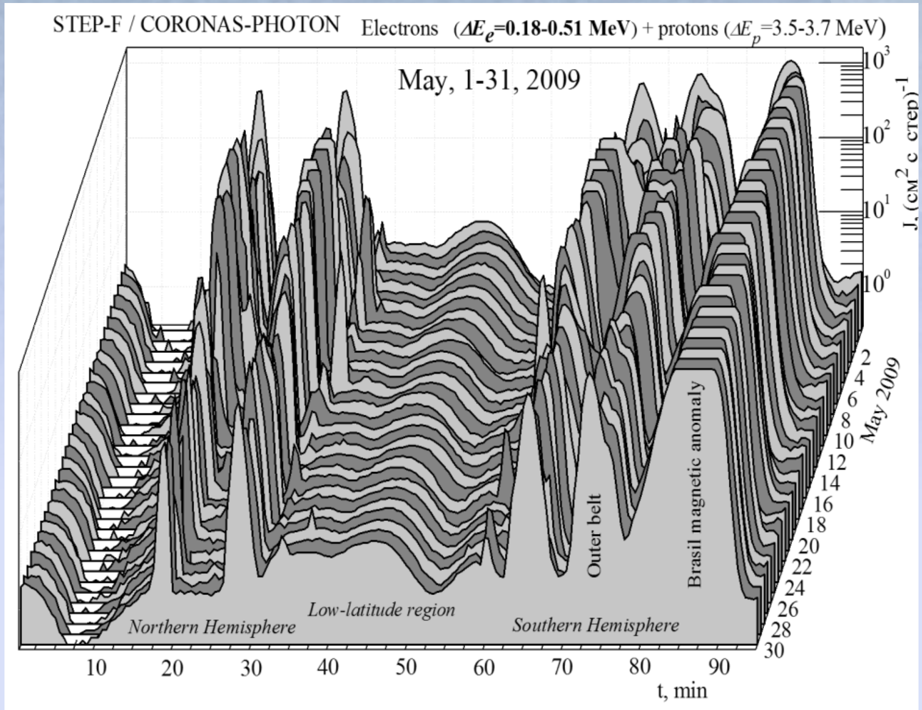

Investigation of electron fluxes at height ~550 km in May, 2009.

Method – comparative observation of particle deviations at one orbit (~96 minutes) from day to day when the satellite pass the same space coordinates

1st orbit from the start of the day is selected for analysis ;

It is clear seen 3 zones of enhanced radiation :

inner belt (seldom appeared); outer belt, and South Atlantic Anomaly

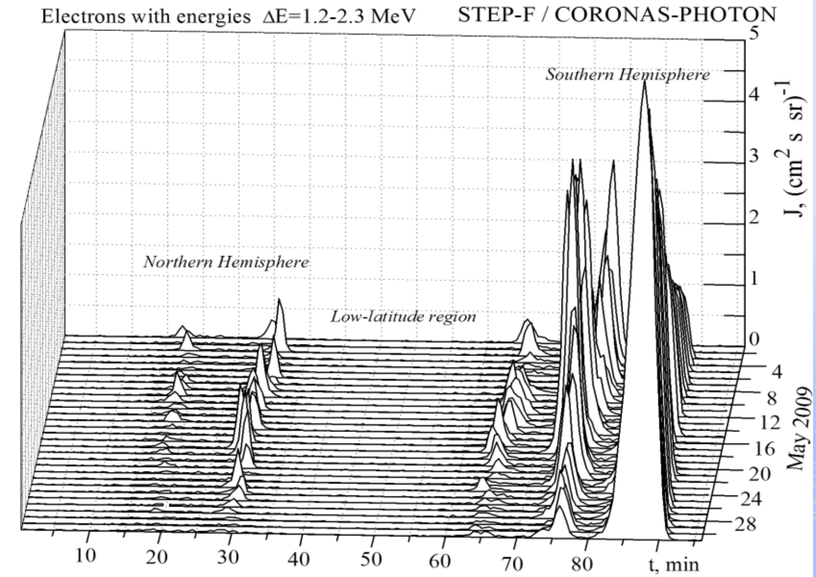

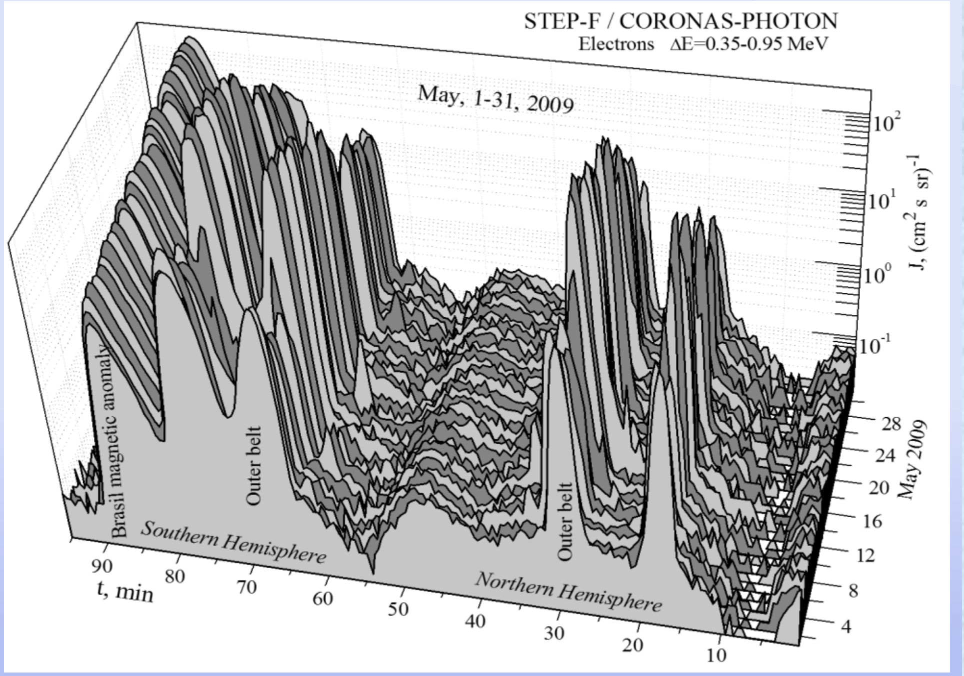

One more approach

Coupling of every-diurnal' particle fluxes during one 96-minutes' orbit from 15 diurnal ones (OY axis) for the period since 1st to 31st May, 2009 (OX axis) - *electrons (0.18-0.51 MeV)+protons (3.5-3.7 MeV)*

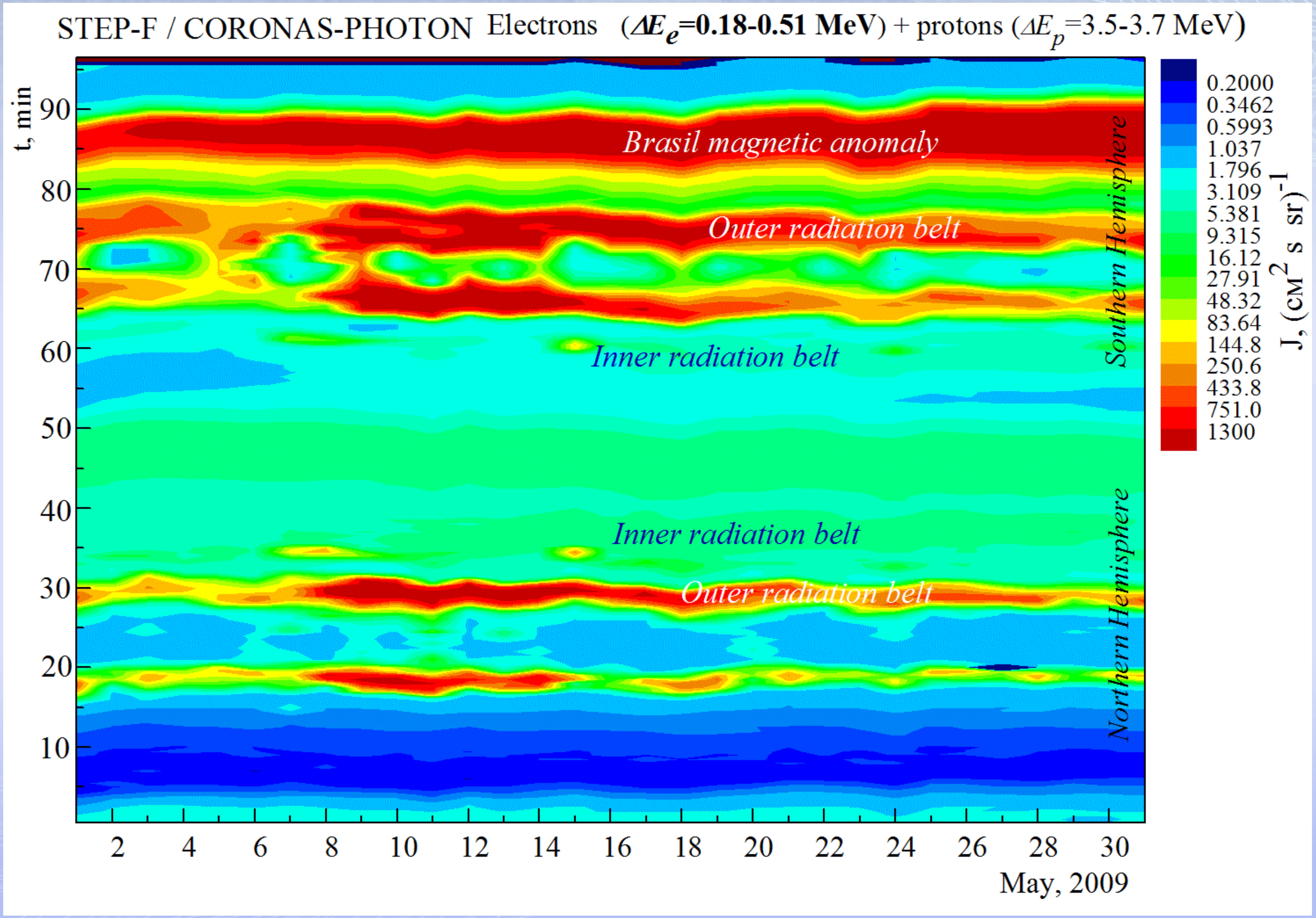

Coupling of every-diurnal' particle fluxes during one 96-minutes' orbit from 15 diurnal ones (OY axis) for the period since 1st to 31st May, 2009 (OX axis) - *electrons (0.35-0.95 MeV)*

It looks like lifetime of electrons in outer belt is some shorter then for electrons with lowest energies;
In the inner belt electrons are almost absent; it may mean that the energy spectrum of inner belt' electrons is falling down quite quick

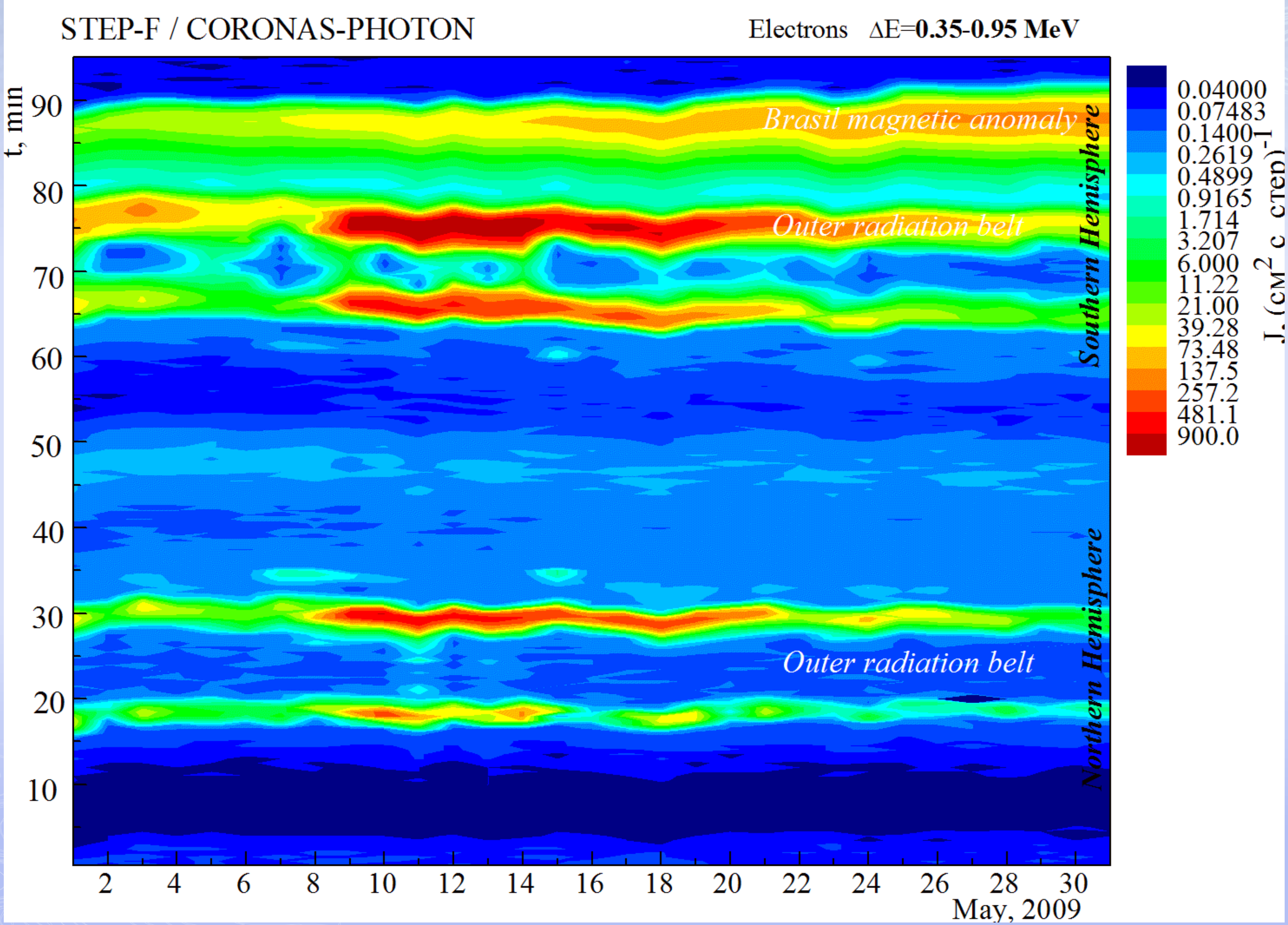

Some conclusions from previous pictures:

1. Non-zero low energy electron fluxes exist everywhere on all latitudes and longitudes , but not only below radiation belts and in the region of South Atlantic magnetic Anomaly (SAA) , and they are preferably anisotropic ones.
2. Significant fluxes in the outer belt at the height s ~550 km are observed at the time of geomagnetic storm and sub-storm as well as during geomagnetically quite periods, while electron fluxes in the inner belt outside of SAA zone are observed as a rule during the storms and sub-storms.

ONE MORE APPROACH TO SEE FEATURES IN PARTICLE FLUXES

Coupling of every-orbit' particle fluxes during 48-minutes' half-circuit (OY axis) for each day

- *electrons (0.18-0.51 MeV) + protons (3.5-3.7 MeV)*

Ascending nodes of the orbit

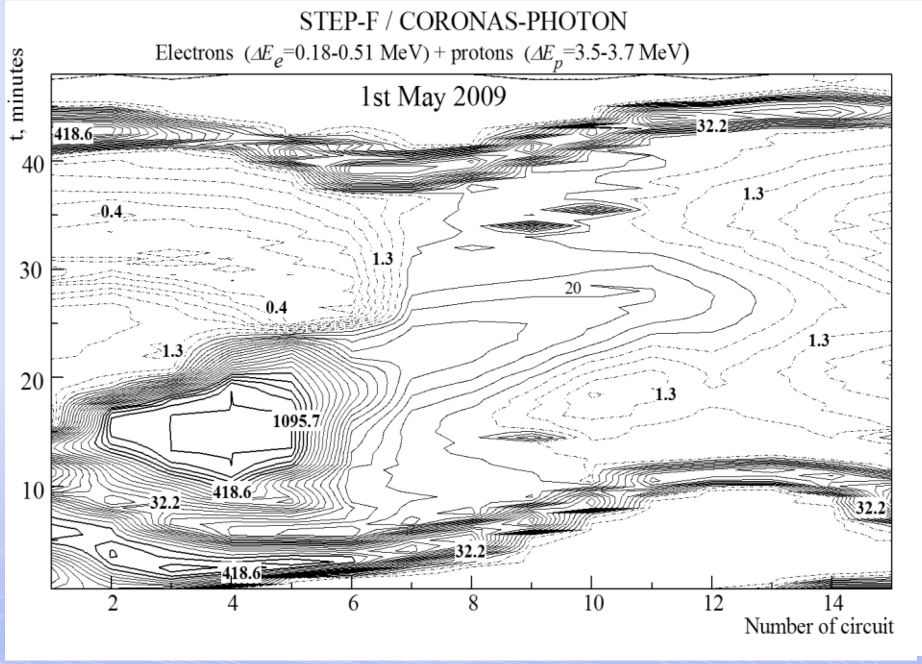

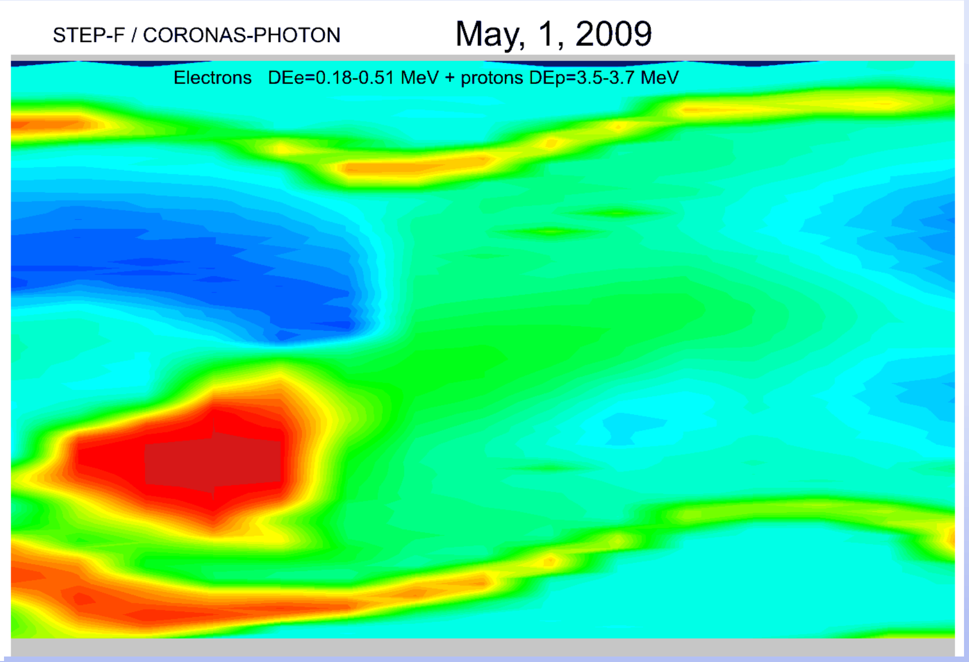

1. Low energy electrons with energies E> 180 keV exist everywhere at the altitudes ~500 km, not depending on latitudes and longitudes
2. There are 3 radiation belts in the Earth' magnetosphere. The 3rd belt is visible on the longitudes that are not coincide with the placement of South Atlantic Anomaly
3. The intensity of all radiation belts at the altitudes ~550 km is very sensitive to the level of geomagnetic activity.
4. The main species of registered electron fluxes is precipitating particles, at least outside of South Atlantic Anomaly.

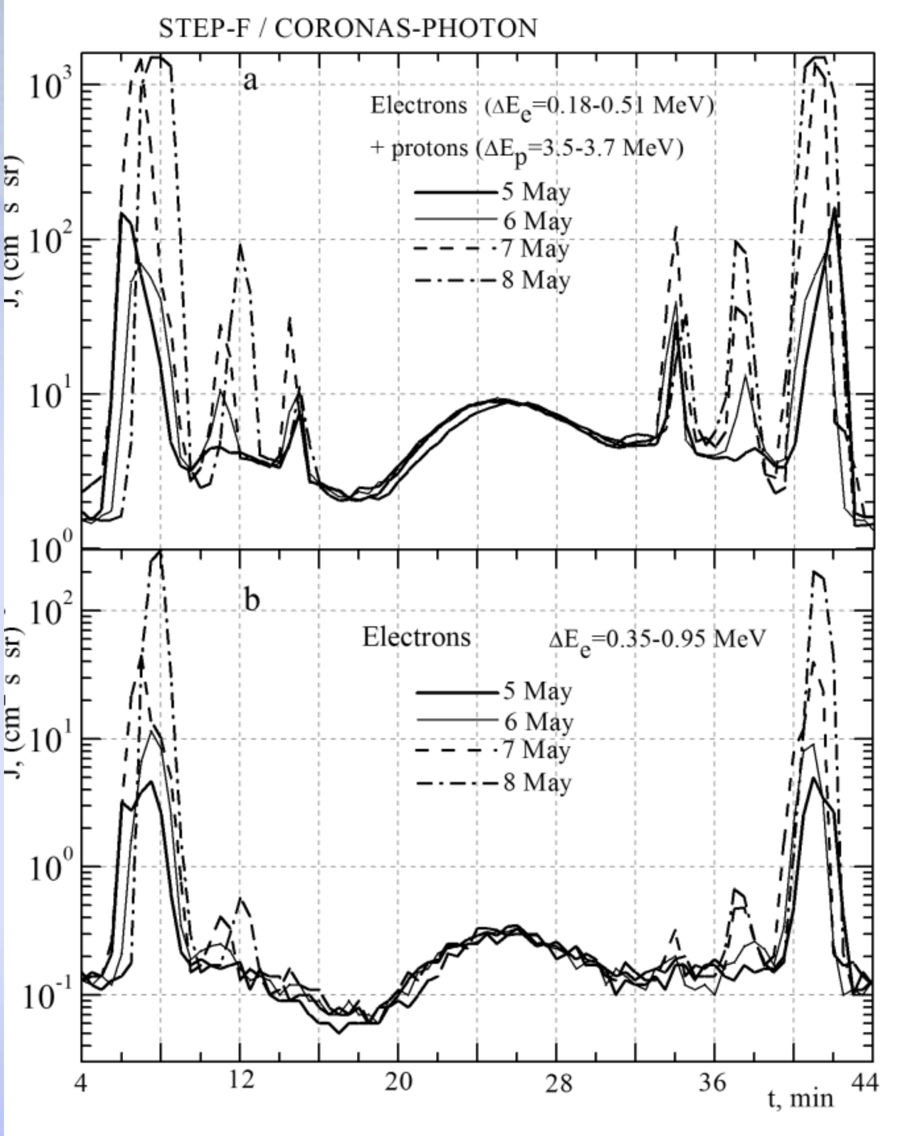

Dynamics of electrons in 3 belts - movie

9th orbit since the start of the day , ascending node, Northern hemisphere

Temporal averaging is 30 seconds. May, 2009

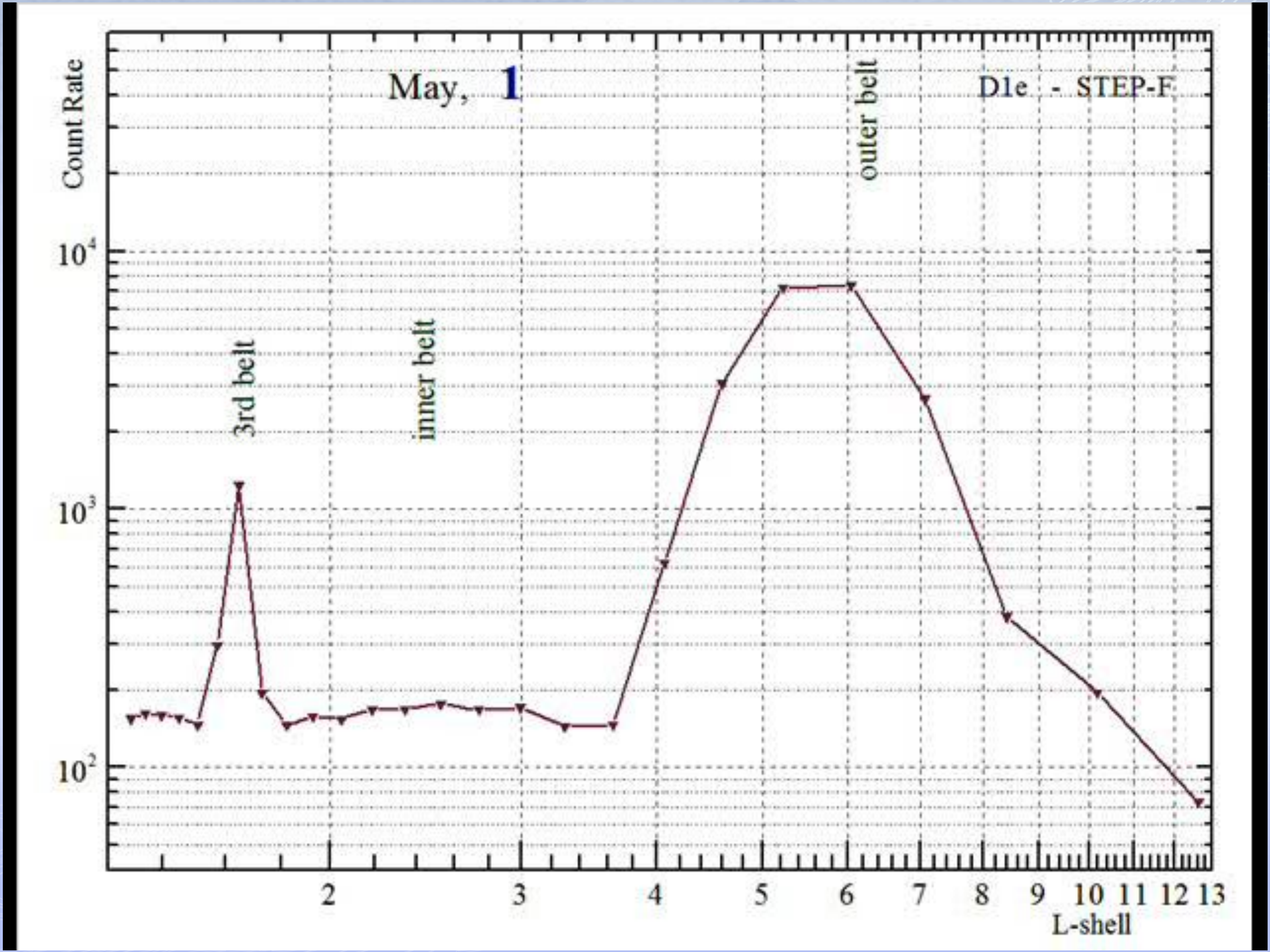

Radiation map in dynamics since 1st May to 10th May,2009

Ascending nodes, Northern hemisphere, time resolution is 30 seconds

Color gamma is for high count rate

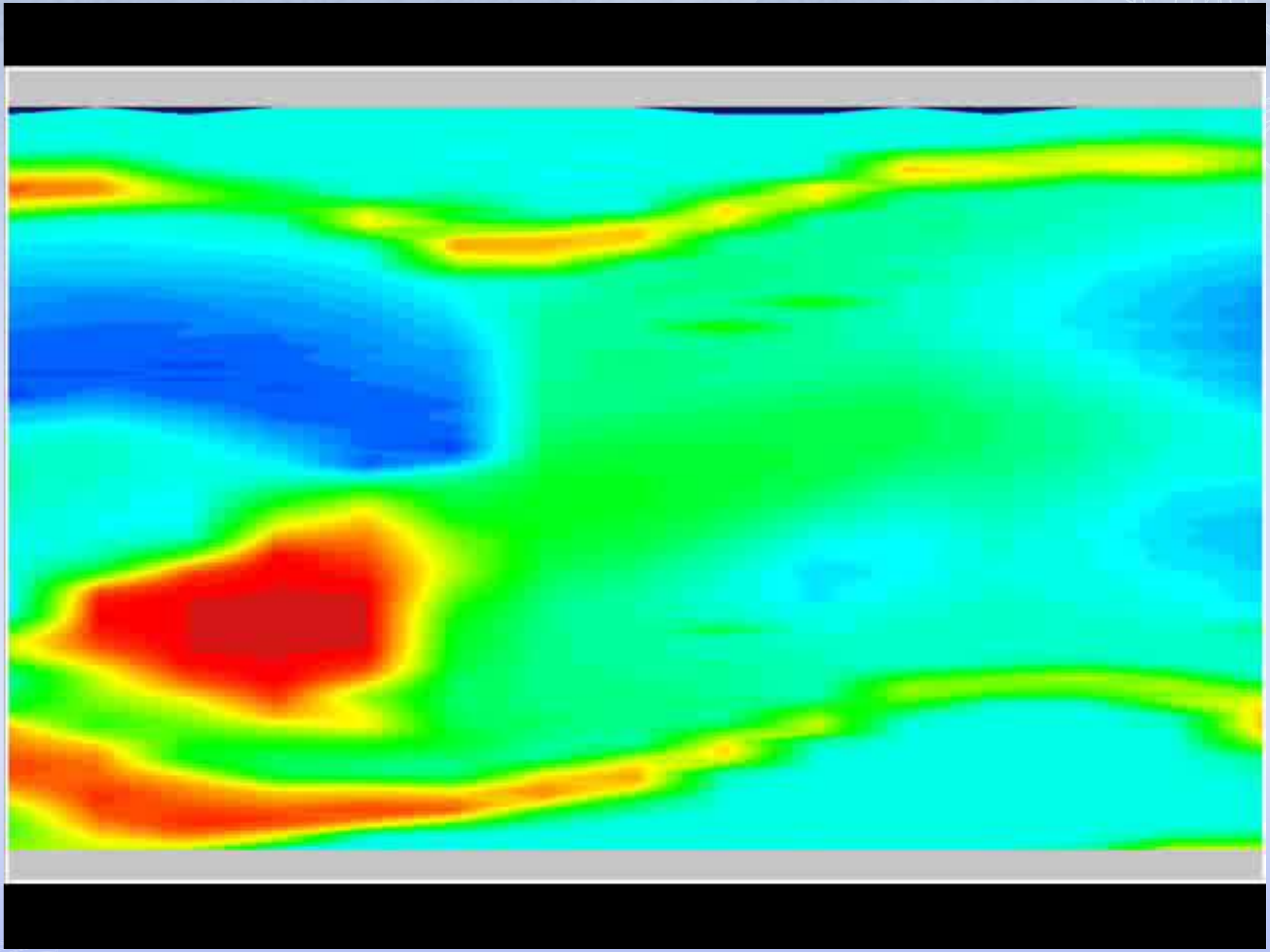

The same , but color gamma is for low count rates

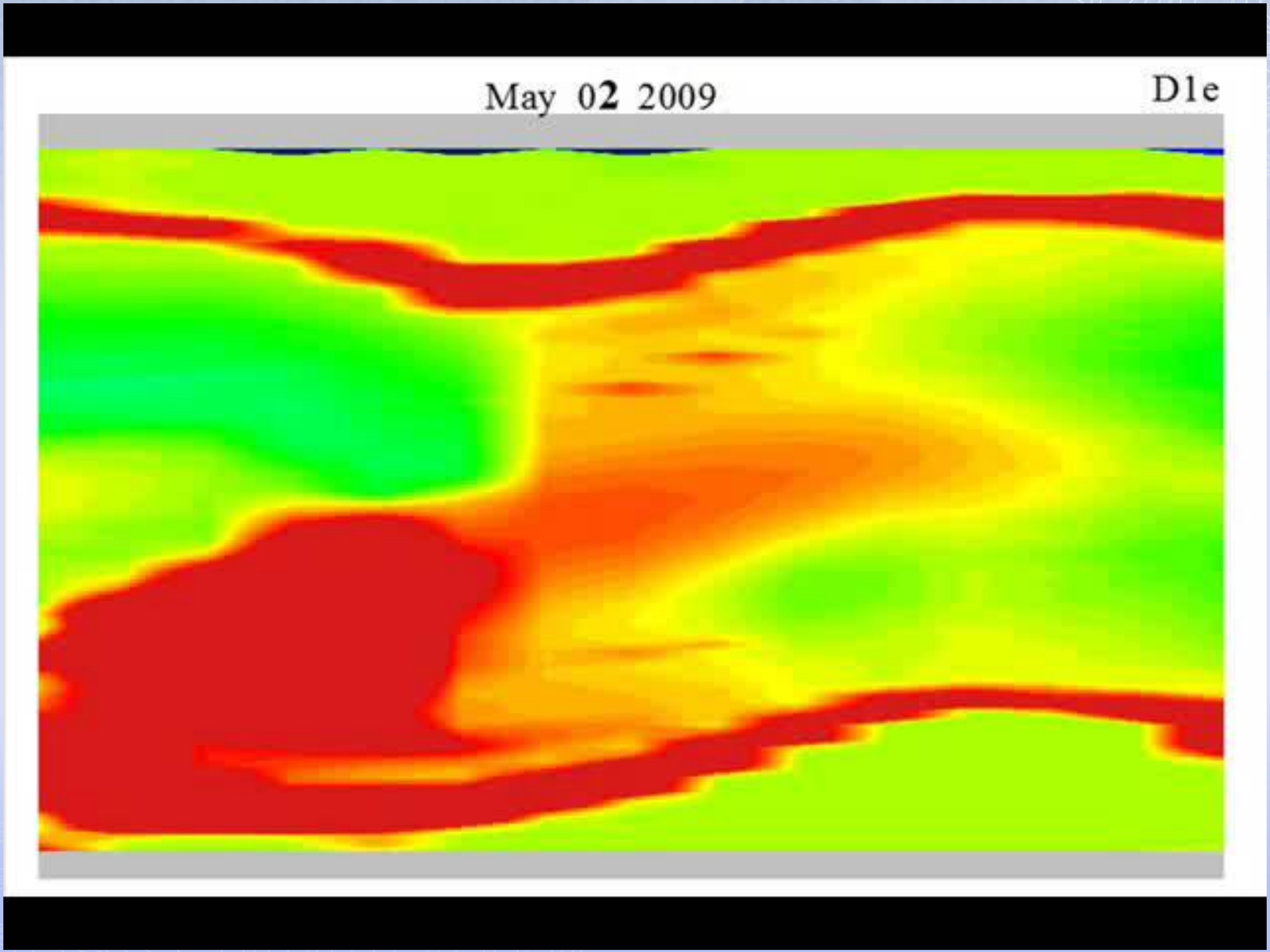

Thank you for your attention!